Paulo Jorge Baeta Mendes

H-O (H-N) COMPLEXES IN METALS, STUDIED BY PERTURBED ANGULAR CORRELATIONS

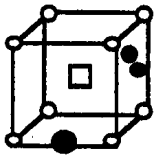

University of Coimbra

1987

INDEX

ABSTRACT

Studies of the interaction of hydrogen and deuterium with the interstitial impurities oxygen and nitrogen in niobium and tantalum were performed using the perturbed angular correlation technique with 181Hf as probe atom.

The interactions due to oxygen and nitrogen in these metals were identified and their evolution as a function of temperature was studied. For oxygen in niobium and tantalum and for nitrogen in tantalum no complexes of more than one interstitial atom were observed for the low concentrations studied. However two different types of complexes were observed for nitrogen in niobium which were attributed to the loading method used for this interstitial.

The relative values of the interaction parameters are interpreted in terms of the valence charge distribution of the impurities. The largest temperature dependence of the asymmetry parameter η in niobium is justified by the fact that the 181Ta atom where the angular correlation is observed is an impurity in niobium whereas in tantalum is similar to the lattice atoms.

The interactions due to oxygen-hydrogen complexes in tantalum and niobium and to nitrogen-hydrogen complexes in tantalum were also identified and their evolution with temperature studied. Similar interactions are observed when deuterium is used instead of hydrogen.

The use of this method confirms that only one hydrogen atom is captured by oxygen or nitrogen in these metals. Using a simple point charge model it was also possible to confirm the position of the trapped hydrogen atom at two neighbouring tetrahedral positions which are fourth nearest neighbours to the oxygen or nitrogen atoms. The probe atom, which is an impurity in these metals, plays an important role on the behaviour of the complexes studied lowering the temperature at which the interactions due to these complexes disappear.

A trapping model in which after the decay of hafnium hydrogen is released and diffuses around the trapping impurity is presented. The values for the mean time of stay of hydrogen obtained with this model lie between those predicted by an extrapolation of the Arrhenius behaviour of the experimental values for the pure metal and for the metal with oxygen or nitrogen as impurities.

A C K N O W L E D G E M E N T S

The present work was made possible only by the encouragement and support of all the members of the Applied Nuclear Physics Group, part of Linha 2 of the Centro de Física da Radiação e dos Materiais of the University of Coimbra, whose creation is due to Prof. Doutor Nuno Ayres de Campos with the collaboration of Prof. Doutor Adriano Pedroso de Lima.

I wish to express my gratitude especially to the following:

Prof. Doutor Nuno Ayres de Campos who selected the research theme and for his constant support and continuous encouragement and friendship,

Prof. Doutor Adriano Pedroso de Lima for his support throughout the work and for his patient and careful reading of the text.,

Prof. Doctor Eckehard Recknagel for granting me access to all the facilities of his laboratory in the Physics Department of the University of Konstanz,

Prof. Doctor Alois Weidinger for his invaluable help in the development of the research and for helpful discussions throughout the work,

Prof. Doutor José Carvalho Soares for the use of his facilities in Lisboa for some low temperature measurements,

to my colleagues in Coimbra, Konstanz and Lisboa,

Deutscher Akademischer Austauschdienst (D.A.A.D.) and the Instituto Nacional de Investigação Científica (I.N.I.C.) for their financial support.

CHAPTER 1

INTRODUCTION

1.1 - The project

This work is the first application of the perturbed angular correlation technique to the study of complexes of hydrogen trapped at interstitial impurities in metallic lattices. The study of these complexes is of great importance particularly in hydrogen diffusion studies in metals. Hydrogen diluted in a perfect metallic lattice has properties similar to those of a gas with a gas phase (α phase), a liquid phase (α‘ phase) and ordered solid phases which depend on temperature as well as hydrogen concentration. The amount of hydrogen which remains in the α phase when the temperature is lowered is drastically reduced due to precipitations in ordered phases. For this reason diffusion measurements at low temperatures are extremely difficult to perform and the diffusion coefficients for hydrogen and it’s isotopes are only known above 120K. A large number of experimental studies have shown that at low temperatures oxygen and nitrogen are good trapping centers for hydrogen in niobium and tantalum. The trapping of hydrogen by nitrogen in niobium has been particularly well studied [Pfeiffer 76, Chen 76, Hanada 77 and 81a, Sado 82, Okuda 84] using methods such as electrical resistivity

and internal friction. It was found that for these systems and at low temperatures N-H (or O-H) complexes are formed while trapping centers are available and that the excess hydrogen atoms precipitate. The internal friction relaxation peaks observed suggest that hydrogen diffuses around nitrogen or oxygen trap centers. This shows that the study of hydrogen diffusion processes at low temperatures is possible by studying it's local diffusion around immobile trap centers as long as the binding energy between hydrogen and the trapping center is high enough to prevent precipitation.

The local diffusion of hydrogen in O-H and N-H complexes in niobium and tantalum has been studied by internal friction [Baker 73, Mattas 75, Schiller 75, Poker 79, Zapp 80a and 80], heat capacity [Morkel 78, Wipf 84], thermal conductivity [Locattelli 78] and neutron spectroscopy [Wipf 81, Magerl 83 e 86]. This studies suggest that hydrogen is located at two neighbouring lattice positions (tetrahedral or quasi-tetrahedral) jumping between them by tunneling. Both oxygen and nitrogen are located at octahedral interstitial positions in niobium and tantalum and the most likely positions for trapped hydrogen is in the pair of tetrahedral positions which are 4^{th} nearest neighbours (4NN) to oxygen or nitrogen. When the temperature is increased hydrogen diffuses around the trapping center jumping to the other 4NN possible positions. If the energy available is enough then hydrogen moves away from the impurity and diffuses through the metal.

Microscopic methods such as perturbed angular correlations overcome some of the limitations of the refered macroscopic methods. It´s local character (defects which are more than three or four unit cells away from the probe are not detected) allows an easy distinction between different types of defects and even between different configurations of the same defect. With this technique measurements of the mean time of residence of hydrogen in

tantalum at temperatures below 30K were first performed by Weidinger and Peichl [Weidinger 85].

In the present work the perturbed angular correlation technique was used to study the trapping and local diffusion of hydrogen and deuterium around oxygen and nitrogen in niobium and tantalum.

1.2 - Plan of thesis

Some of the fundamental aspects of the perturbed angular correlation method used in this work are presented in chapter 2. A summary of the theory of angular correlations and of the hyperfine interaction between the nuclear quadrupole moment and the external electric field gradient is presented in appendix A. The properties of the nuclear probe used as well as the point charge model for electric field gradient calculation are also presented.

In chapter 3 the experimental systems and the methods used to dilute the probe atoms, oxygen, nitrogen, hydrogen and deuterium are described. The hydrogen concentration measurement system developed is also discussed as well as the numerical methods used in the data analysis. In appendix B the data acquisition system developed in Coimbra is presented.

The studies of oxygen and nitrogen interactions in niobium and tantalum are presented in chapter 4. The interactions observed are identified and the temperature dependence of their parameters are discussed for the different systems. At the end of this chapter a summary of the relevant conclusions is made.

The results of the studies of the interaction of hydrogen with oxygen and nitrogen in tantalum and with oxygen in niobium are presented in

chapter 5. The different interactions present are identified and the dependence on temperature of the fraction of trapped hydrogen atoms s interpreted in terms of trapping models. The limitations of several models are discussed and a summary of conclusions is presented at the end of the chapter.

Finally in chapter 6 some final remarks are made and future developments are suggested.

CHAPTER 2

THEORETICAL CONSIDERATIONS

2.1 - Hyperfine interactions

The interaction of the nuclear charge distribution with the electromagnetic fields produced either by the atomic electrons or by the crystal charges, hyperfine interactions, induce changes in the nuclear and atomic energy levels. The hyperfine interaction Hamiltonian may be conveniently written in terms of a multipolar expansion:

$$H_{hi} = H(E0) + H(M1) + H(E2) + \ldots \qquad (2.1)$$

where H(E0) is the electric monopole term, H(M1) is the magnetic dipole term, H(E2) is the electric quadrupole term, etc. and correspond to the nuclear moments which do not vanish due to symmetries of the nuclear states.

Each term of the expansion of H_{hi} may be written as a product of a nuclear moment and a corresponding electromagnetic moment. Therefore hyperfine interaction studies give information concerning nuclear moments or crystal fields. However the experimental determination of either of the two terms requires a detailed knowledge of the other.

Studies of hyperfine interactions may be carried out by several methods wether in ground states of stable nuclei, or with half-lives of the order of several minutes (high resolution optical spectroscopy, nuclear magnetic

resonance(NMR)), or in nuclear excited states (Mössbauer spectroscopy, perturbed angular correlations (PAC)). These last methods use nuclear radiation to detect the hyperfine interaction and are nowadays considered as very powerful tools in different research fields such as Solid State Physics, Chemistry and even Biology.

In the perturbed angular correlation method used in this work the hyperfine interaction between the nuclear quadrupole moment and the electric field gradient due to the atomic and crystalline charge distribution is studied. The general theory of angular correlations and hyperfine interactions is well known and only a brief summary is presented in Appendix A.

2.2 - The perturbed angular correlation

The perturbed angular correlation method consists basically in obtaining an ensemble of aligned nuclei in an excited state and measuring the angular distribution of the radiation emitted from this state. Alignment of an ensemble of nuclei is obtained when the population of different magnetic sub-states are not equal but states with symmetric magnetic quantum numbers, $\pm m$, are equally populated.

When the nucleus decays by the successive emission of two γ rays in a cascade as shown in Fig.2.1, detecting γ_1 in a fixed direction k_1 selects an aligned ensemble of nuclei and the radiation γ_2 shows an angular correlation relative to k_1.

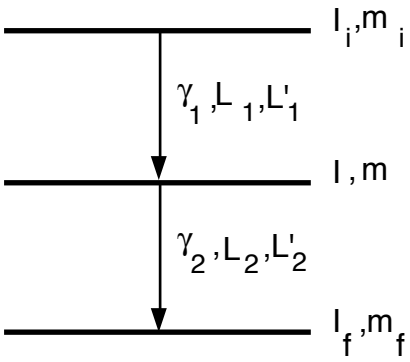

Fig. 2.1- Decay cascade of an excited nucleus. The nucleus decays from the level (I_i,m_i) to the level (I_f,m_f) by the emission of two γ rays γ_1 and γ_2 successively through the intermediate state (I,m). The multipolarity of the radiation is L_1 and L_2.

The interaction between the external electromagnetic field and the nuclear moments of the intermediate state I is present only during the time between it's formation and successive decay. The effect of this interaction on the angular correlation may be understood, in a semi-classical picture, if we consider that due to the interaction of the nuclear moments with the external electromagnetic field moments, the nucleus in it's intermediate state I precesses around the quantization axis defined by the external field. This precession will cause the angular correlation to change with time. From the quantum point of vue the hyperfine interaction induces periodical transitions between states with different magnetic quantum numbers m, changing the population parameters of the initial state and therefore the angular correlation.

The perturbed angular correlation method using radioactive sources has been extensively used for the measurement of electric field gradients in the study of crystalline fields [Witthuhn 83] and in the study of defects in materials [Recknagel 83].

For a polycrystalline sample and in a cylindrical symmetry the perturbed angular correlation may be written as:

$$W(\theta,t) = \sum_{k=0}^{k_{max}} A_{kk}\ G_{kk}(t)\ P_k(\cos\theta) \qquad (2.2)$$

where k is even and

- k_{max} is the smallest of $(2I, L_1+L'_1, L_2+L'_2)$ where I is the spin of the intermediate state and L_1, L'_1, L_2 and L'_2 are the multipolarities of γ_1 and γ_2 (Fig.2.1). When only one multipolarity is observed for each radiation k_{max} is the smallest of $(2I, 2L_1, 2L_2)$.
- A_{kk} are the anisotropy constants characteristic of the decay and which depend on the spins and multipolarities involved. They are tabulated for instance in [Frauenfelder 65],
- $G_{kk}(t)$, the perturbation factors, contain all the information regarding the hyperfine interaction of the intermediate state I with the external field,
- $P_k(\cos\theta)$ are the Legendre polynomials of order k.

For the case of the hyperfine interaction between the nuclear electric quadrupole moment with an external electric field gradient with axial symmetry the perturbation factor in (2.2) is given by:

$$G_{kk}(t) = \sum_{n=0}^{n_{max}} s_{kn} \cos(n\,\omega_0\,t) \qquad (2.3)$$

Where ω_0 is the smallest precession frequency which can be observed (see (A.38)) and n_{max} depends on the spin of the intermediate state. The coefficients which correspond to the transition probabilities between the hyperfine levels are defined by (A.44) and are tabulated for several spin values in [Frauenfelder 65].

When the electric field gradient is not axial symmetric the transition probabilities and energies are a function of the asymmetry parameter η (defined below) and the perturbation factor becomes:

$$G_{kk}(t) = \sum_{n=0}^{n_{max}} s_{kn}(\eta) \cos(n_n(\eta)\,\omega_0\,t) \qquad (2.4)$$

where $n_n(\eta)$ is the ratio between the experimental frequencies, ω_n, and the frequency w_0 for η=0.

2.3 - The electric quadrupole interaction

After a suitable transformation to the principal axes the electric field gradient tensor which interacts with the nuclear quadrupole moment may be characterized by two parameters; the component with the largest absolute value V_{zz} and the asymmetry parameter η defined by (see App.A):

$$\eta = \frac{V_{xx} - V_{yy}}{V_{zz}} \quad ; \quad 0 \le \eta \le 1 \qquad (2.5)$$

and which gives the deviation of the field gradient tensor from the axial symmetric case where $V_{xx} = V_{yy}$.

The interaction is proportional to the product of the two tensors [Matthias 63] causing a splitting of states with different |m|.

For the simple case of an axially symmetric electric field gradient (η=0) the energy differences between the states m and m' is:

$$\Delta E = E_m - E_{m'} = 3\,\omega_Q\,h \vee m^2 - m'^2 \vee \qquad (2.6)$$

where we define the quadrupole interaction frequency by:

$$\omega_Q = \frac{e\,Q\,V_{zz}}{4I\,(2I+1)\,h} \qquad (2.7)$$

The strength of the quadrupole interaction may be expressed by the interaction frequency:

$$\nu_Q = \frac{e}{h}\,Q\,V_{zz} \qquad (2.8)$$

which is independent of the intermediate level spin.

When the field gradient is not axial symmetric ($\eta \neq 0$) the influence of η on the energies of the m-states may be easily understood if we write the quadrupole interaction Hamiltonian as a function of the angular momentum operators:

$$H = \frac{e\,Q\,V_{zz}}{4I\,(2I+1)}\left[3I_z^2 - I^2 + \frac{\eta}{2}\,(I_+^2 + I_-^2)\right] \qquad (2.9)$$

When $\eta \neq 0$ the third term of the Hamiltonian gives non-zero off diagonal elements and it is necessary a numerical diagonalization in order to determine the energies of the m-states. In Fig.2.2 the energy splitting of the m-states due to the quadrupole interaction as a function of η for a nuclear level with spin I=5/2 is presented.

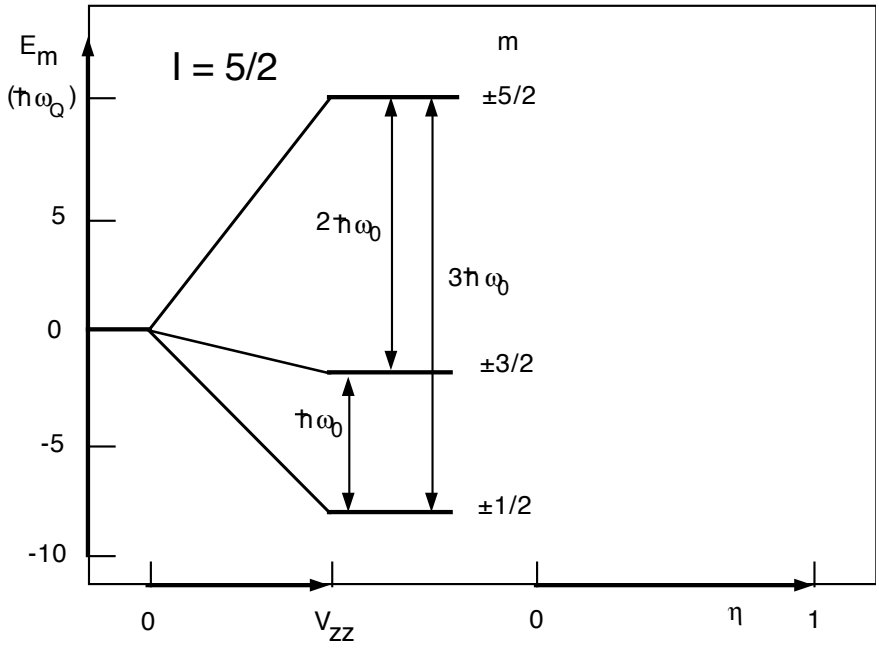

Fig. 2.2- Energy splitting of the m-states of a nuclear level with spin I=5/2 due to the hyperfine quadrupole interaction with an electric field gradient for $\eta=0$ and $\eta\neq0$.

2.4 —The probe nucleus

In order to perform perturbed angular correlation experiments with radioactive sources it is necessary to dissolve the atom probes in the material studied. In this work the atom ^{181}Hf, which decays by β emission to ^{181}Ta, was used. In Fig.2.3 a simplified decay scheme for this nuclide is presented. ^{181}Ta has a γ cascade with an intermediate level with spin I=5/2 and a quadrupole moment Q=2.80barn [NDS 84]. The A_{kk} coefficients have the following values A_{22}=-0.295(5) and A_{44}=-0.068(9) [NDS 73] normalized to the value of A_{00}. As the A_{44} term is very small it's influence is usually not considered and the perturbed angular correlation may be written as:

$$W(\theta,t) \cong 1 - 0.295\, G_{22}(t)\, P_2(\cos(\theta)) \qquad (2.10)$$

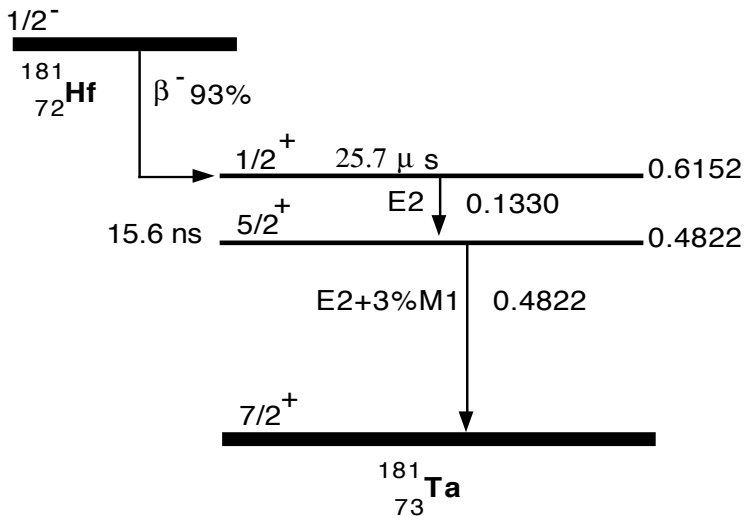

Fig. 2.3- Decay scheme of ^{181}Hf showing the cascade used in the perturbed angular correlation experiments. The times shown are half-lives and the energies are in MeV [Lederer 78, NDS 84].

The perturbation factor, with n taking all integer values from zero up to n_{max}=3, for an axial symmetric field gradient is given by:

$$G_{22}(t) = \sum_{n=0}^{3} s_{2n} \cos(n \omega_0 t) \qquad (2.11)$$

and by:

$$G_{22}(t) = \sum_{n=0}^{3} s_{2n}(\eta) \cos(n_n(\eta) \omega_0 t) \qquad (2.12)$$

for a non-axial symmetric field gradient.

2.5 - The point charge model

As the theoretical determination of the electric field gradient in a metal requires a detailed knowledge of the electronic wave functions of the crystal it is not possible to calculate it exactly even for the simplest metals. The theoretical methods developed for these calculations are usually based in approximations depending on the particular metal in study which difficults their application to other metals.

Furthermore these studies have usually been concentrated in non-cubic metals [Kaufman 79, Vianden 83] and on the calculation of field gradients caused by substitutional impurities in cubic metals at their nearest neighbours [Ponnambalam 84,85, Pal 85, Prakash 85]. Theoretical studies of electric field gradients caused by interstitial impurities in cubic metals are practically non-existent.

Usually two contributions to the electric field gradient are considered, one is due to the electronic charge density outside the atom used as probe and the second is due to non-spherical charge distributions belonging to the probe atom:

$$V_{zz} = (1-\gamma_\infty) V_{zz}^{Ext} + (1-R) V_{zz}^{Loc} \qquad (2.13)$$

The Sternheimer anti-shielding factor γ_∞ gives the enhancement of the field gradient at the nucleus due to the polarization of the probe nucleus electronic shells by the external field gradient. This factor is negative for most ions and has usually values in the range $10 \leq -\gamma_\infty \leq 80$ [Feiock 69]. R is the shielding factor for the local gradient and has usually values in the range $-0.2 \leq R \leq 0.2$ [Kaufmann 79].

As refered above theoretical calculations of electric field gradients use rather elaborate models that are specific for each metal studied. With the use of models the identification of defect configurations is, in principle, possible by comparing the experimental results with the theoretical calculations. However due to the fact that each model must be adapted to the type of defect considered and that the field gradient has to be calculated for all possible defect configurations, these calculations are not feasible from the practical point of vue.

These difficulties have led to the use of a very simple, although rather unrealistic, model for the determination of the electric field gradient; the point charge model. In this model the crystal charge distribution is replaced by point charges placed at the equilibrium lattice points and the field gradient is calculated using this charge distribution. The so called lattice contribution to the electric field gradient, $(1-\gamma_\infty)V_{zz}^{Rede}$, which is often used instead of the first term in (2.13). This value is usually much different from the experimental values. This difference is often attributed to local gradients included on the second term of (2.13). In spite of it's simplicity this model has been successfully used to predict the symmetry of field gradients in the presence of impurities [Weidinger 79, Wrede 86]. An improved version of this model where the crystal electronic charge distribution is also replaced by negative point charges placed in points where this density is greater is sometimes used [Bodenstedt 85, Gil 87b].

In the point charge model the electric field gradient tensor created by the charge distribution external to the probe atom is calculated from the second derivatives of the electrostatic potential:

$$V_{\alpha\beta}^{Rede} = \frac{\partial^2 V}{\partial x_\alpha \partial x_\beta} \qquad (2.14)$$

The potential at the origin due to a point charge Ze at r is:

$$V_i = \frac{1}{4\pi\varepsilon_0} \frac{Ze}{r_i} \qquad (2.15)$$

Calculating the derivatives in (2.14) with the potential in (2.15) and summing for all point charges the electric field gradient tensor is:

$$V_{\alpha\beta}^{Rede} = \sum_i \frac{Ze}{4\pi\varepsilon_0 r_i^5} \begin{bmatrix} 3x_i^2 - r_i^2 & 3x_iy_i & 3x_iz_i \\ 3x_iy_i & 3y_i^2 - r_i^2 & 3y_iz_i \\ 3x_iz_i & 3y_iz_i & 3z_i^2 - r_i^2 \end{bmatrix} \qquad (2.16)$$

After diagonalization and ordering the tensor components according to the

convention $V_{xx}^{Rede} \leq V_{yy}^{Rede} \leq V_{zz}^{Rede}$ the strength of the electric field gradient affecting the nucleus may be calculated

$$V_{zz} = (1-\gamma_\infty) V_{zz}^{Rede} \quad ; \quad \eta = \frac{V_{xx} - V_{yy}}{V_{zz}} \qquad (2.17)$$

A value of $\gamma_\infty \cong -62$ was used for ^{181}Ta obtained by interpolating between the values calculated by Feiock for hafnium and tungsten [Feiock 69].

The interaction frequency ν_Q (2.5) is usually determined in order to compare it with the experimental frequencies observed.

CHAPTER 3

EXPERIMENTAL

3.1 - The experimental system

The experimental set-up for perturbed angular correlation experiments is basically formed by a set of detectors suitable for the radiation used and an electronic system for signal processing and data collection.

3.1.1 - Detectors and electronics

In the experimental system used in this work four detectors at 90° and a fast-slow coincidence system were used. This system allows the collection of eight time spectra and the block diagram of the electronics associated with each detector is represented in Fig.3.1. This geometry allows a compensation of the efficiencies and of small asymmetries on the detector geometries in the analysis of the results (see section 3.3). On the other hand the coincidences between the time and energy signals from each detector lowers the count rate at the time to amplitude converter inputs.

Sodium iodide scintillators (NaI(Tl)) coupled to Phillips XP-2020 photomultipliers were used and a time resolution of the order of 2.6ns was

achieved. In some experiments cesium fluoride (CsF) and barium fluoride (Ba_2F) scintillators also coupled to XP-2020 photomultipliers were used. Using these scintillators has the advantage of achieving a better time resolution allowing a better determination of the interaction frequencies observed. Barium fluoride has the further advantage of a better energy resolution as well as greater efficiency than cesium fluoride. However as the fast component of light emitted by this scintillator is in the ultra-violet region they require the use of photomultipliers with quartz windows (XP-2020 Q). Time resolutions of 1ns and 0,8ns were obtained with cesium fluoride and barium fluoride respectively.

Two signals are produced by the detectors for each γ ray detected, one corresponding to the energy deposited by the radiation on the scintillator (slow signal) and one which defines the time at which the interaction with the detector took place (fast signals). The slow signals are identified by single channel analyzers as being start or stop signals of the relevant cascade. The fast signals are delayed and coincidences with the slow signals are performed. Fast signals which correspond to valid coincidences are mixed in fast OR's and go to the input of the time to amplitude converter. On the other hand logic signals of valid coincidences go to a routing module which identifies the particular combination of detectors responsible for this event.

Of the twelve possible spectra only eight are stored corresponding to four 180° and four 90° angles as shown in Tab.3.1. The main advantage of this particular choice is that it allows a better suppression of crosstalk problems between the fast electronics of detectors 1 and 2 and of detectors 3 and 4. This problem, which causes spurious oscillations in the spectra, is not critical when sodium iodide scintillators are used but becomes important with the faster scintillators cesium fluoride and barium fluoride.

Tab. 3.1- Detector combinations and angles angles *f*or the spectra collected in the multichannel analyzer.

Detectors		Angles
1	3	180
1	4	90
2	3	90
2	4	180
3	1	180
3	2	90
4	1	90
4	2	180

The routing module is not available commercially and had to be made for the purpose. It's block diagram is shown in Fig.3.2. On it's output this module gives a valid coincidence signal and a 3 bit word containing information on the detector combination responsible for the time to amplitude conversion. The coincidence signal is present only when the detector combination is valid and only one start and one stop signal were received at the routing inputs. The 3 bit word is added to the analog to digital converter word and route this conversion to different memory regions of the multichannel analyzer. The time during which the routing word is available for the multichannel analyzer is controlled by the time to amplitude converter's true start and true stop outputs.

The block diagram of the experimental set-up used in Coimbra is represented in Fig.3.3. This system does not use fast-slow coincidences which reduces the number of modules needed. Furthermore as only four single channel analyzers were available detectors 1 and 2 and detectors 3 and 4 only detected start and stop signals respectively and only the first four combinations of Tab.3.1 are accumulated. Recently the addition of four sin-

gle channel analyzers made possible the use of all eight spectra combinations.

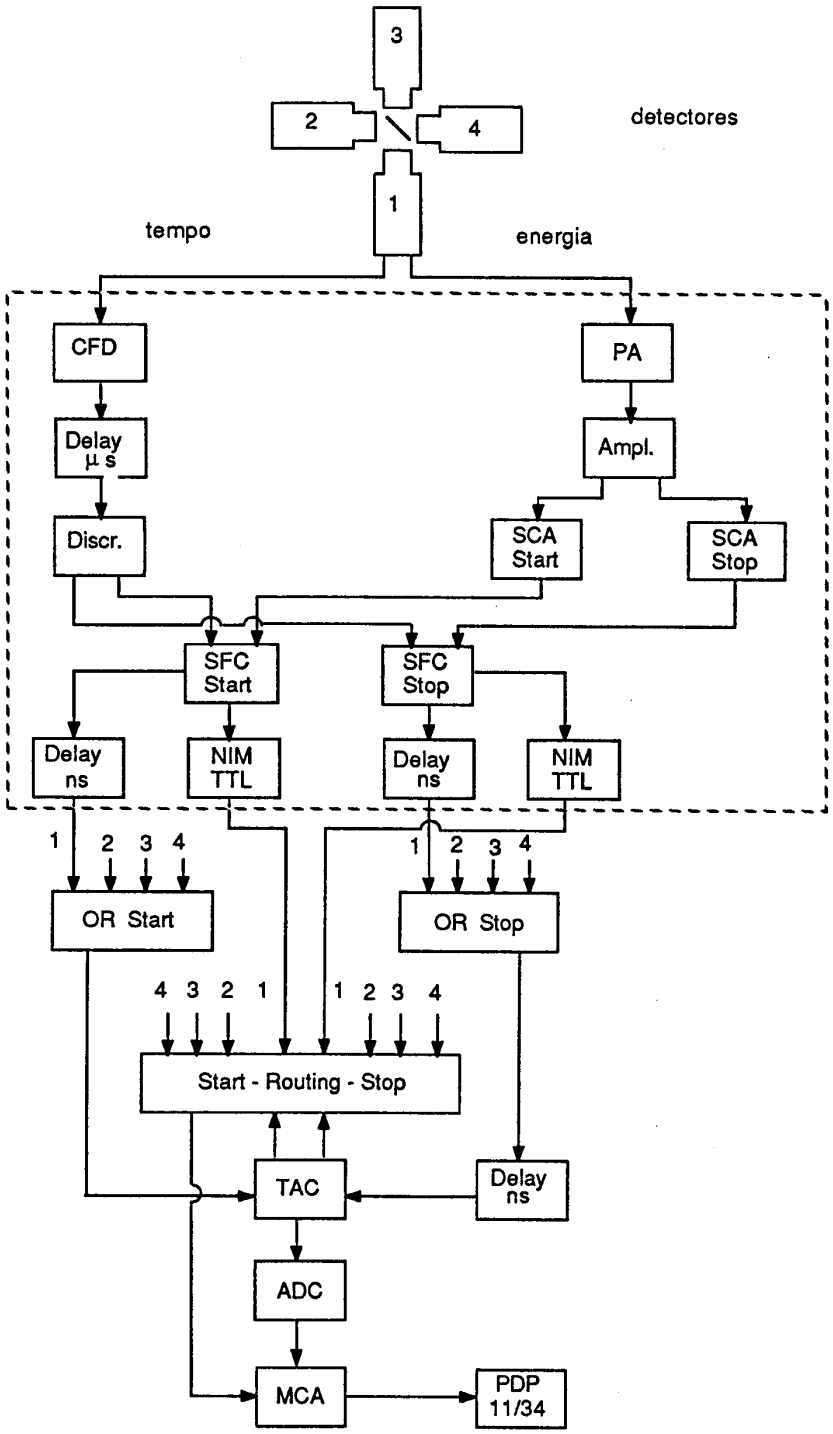

Fig. 3.1- Block diagram of the electronics for the perturbed angular correlation set-up. The modules within the rectangle are repeated for each detector: CFD- constant fraction discriminator, Delay (μs)- long delay for fast signals (RG-213/U), Discr- discriminator, PA- pre-amplifier, Ampl- amplifier, SCA- single channel analyzer, SFC- fast coincidences, NIM/TTL- NIM/TTL converters, Delay(ns)- delay, OR- fast OR, Routing- routing module, TAC- time to amplitude converter, ADC- analog to digital converter, MCA multichannel analyzer.

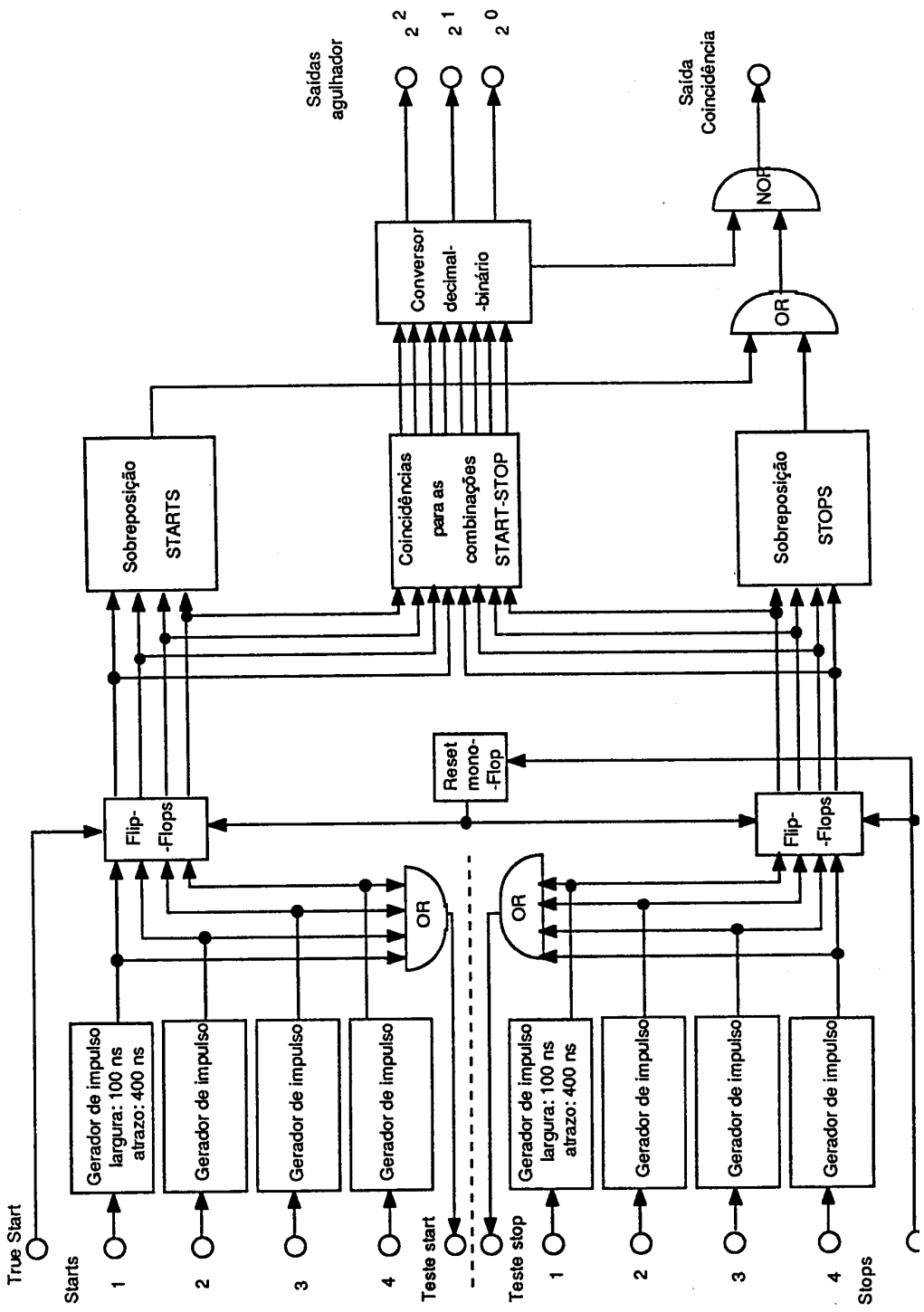

Fig. 3.2- Block diagram of the routing module

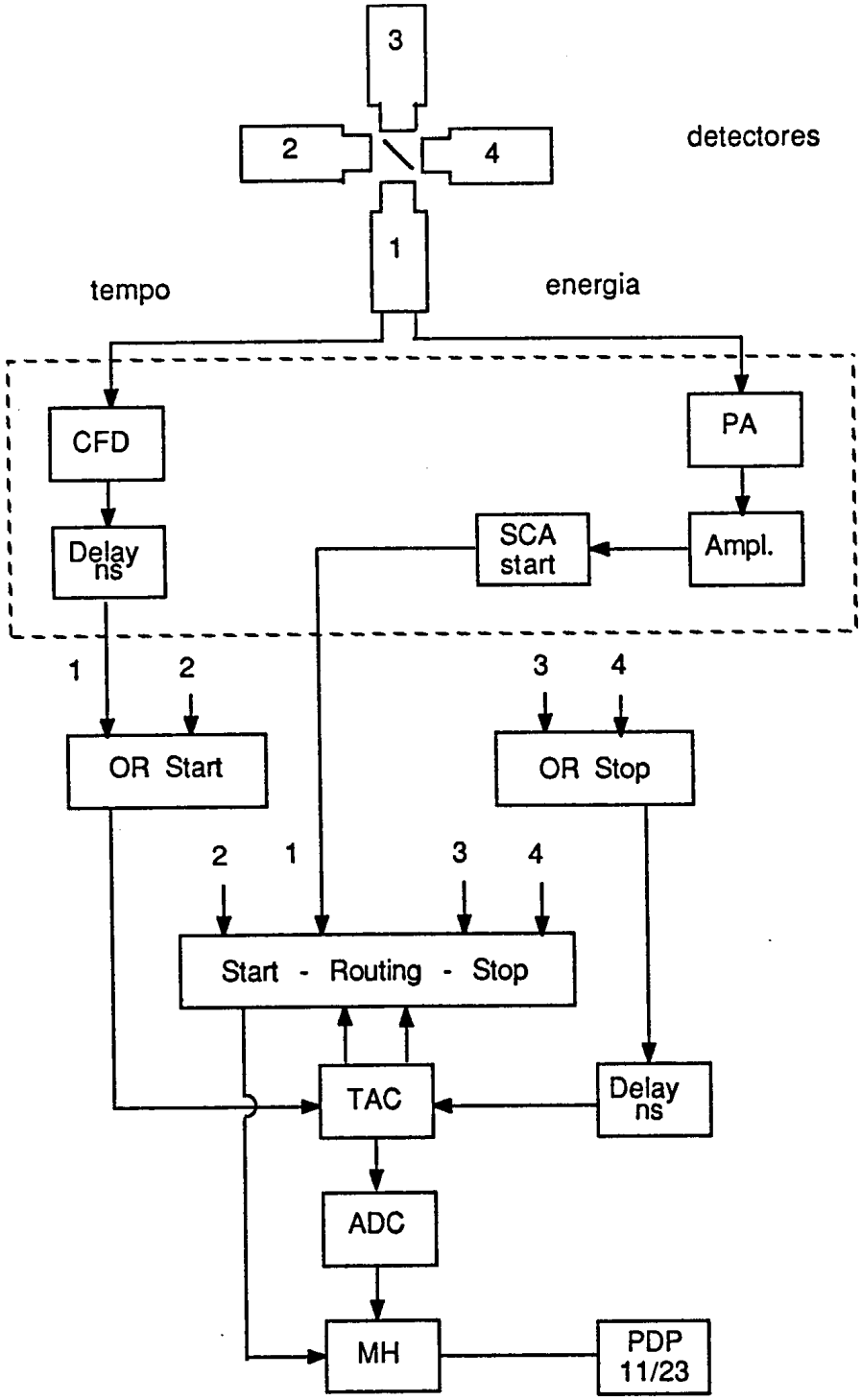

Fig. 3.3- Block diagram of the electronics for the perturbed angular correlation set-up used in Coimbra. This system does not use the fast-slow coincidence circuit of the previous set-up. The modules within the rectangle are repeated for each detector: CFD- constant fraction discriminator, Delay(ns)- delay, PA- pre-amplifier, Ampl- amplifier, SCA- single channel analyzer, OR- fast OR, Routing- routing module, TAC- time to amplitude converter, ADC- analog to digital converter, MH- histogramic memory.

The detectors used in this system consist of sodium iodide scintillators coupled to XP-2020 photomultipliers and a time resolution of 2.7ns was achieved.

Besides the perturbed angular correlation experiments also positron annihilation experiments are performed in Coimbra. Therefore a modular data acquisition system with independent analog to digital converters was developed. The acquisition process is controlled by a computer thru an appropriate CAMAC interface. This system is described in Appendix B.

3.1.2 - Cryostat and temperature control

All measurements were made in the temperature range between 8K and 300K. To achieve these temperatures the samples were placed in a closed cycle helium cryostat. The temperature is controlled by a high precision PID controller with an uncertainty of ±0.2K. In Fig.3.4 the sample holder is represented.

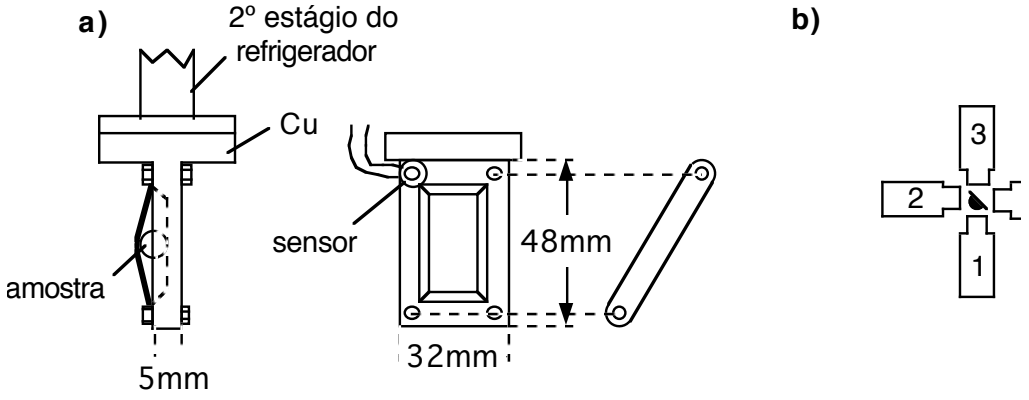

Fig. 3.4- a) Sample holder for the closed cycle helium cryostat.
b) Relative position of the sample holder and the detectors in order to minimize self-absorption.

3.2 Sample preparation

3.2.1 - Probe atom dilution

As was previously refered to perform perturbed angular correlation experiments in metals it's necessary to dilute the radioactive probe in the metal studied. In metals this dilution depends on the metal affinity to form alloys with the radioactive species.

In the present work ^{181}Hf was used as radioactive probe as it presents several advantages for these studies: Hafnium is soluble in metals of the vanadium group [Moffat 78] and since it occupies substitutional places in the cubic lattice the electric field gradient is zero in the absence of other defects; on the other hand the fact that the recoil energy of the β decay of ^{181}Hf to ^{181}Ta (approximately 2eV) is much smaller than the average energy necessary to move a lattice atom to an interstitial position (typically 25eV [Nelson 75]) the radioactive ^{181}Ta remains in the same position as it's parent nucleus. When studying tantalum, hafnium has also the advantage of being transformed into a lattice atom by the decay leaving the lattice unperturbed. The half-life of ^{181}Hf is 42.4 days which allows several months for measurements. Also the activated ^{181}Hf is very easy to obtain by irradiating in a reactor natural hafnium according to the reaction ^{180}Hf(n,γ) ^{181}Hf.

The hafnium for irradiation (approximately 1mg) is encapsulated in a quartz ampoule to facilitate transport and irradiation. The activation was done at the Kernforschungsanlage Jülich with a thermal neutron flux of 10^{15} n/cm^{2}s during approximately two months and the specific activity reached was of the order of 200mCi/mg. One disadvantage of this nuclide is the fact that the irradiated hafnium is still essentially inactive (for the

specific activities reached only 10% of the atoms are activated) and as, in general it is not possible to separate the activated atoms we must dilute a high fraction of inactive hafnium in the metal.

The dilution of the radioactive species in the metal may be performed by either of the three following methods: diffusion, implantation or melting of the two metals. As the diffusion coefficients of hafnium in tantalum and niobium are very small the diffusion method can not be used. Implantation raises some technical problems specially the strong and persistent contaminations of the accelerator due to the long half-life of ^{181}Hf. The samples were therefore prepared by melting together tantalum and niobium of 99.96% purity, both from Materials Research Corporation, and irradiated hafnium (96.6% Hf, 3.3% Zr). Melting was performed in an electron gun in ultra-high vacuum

Tab. 3.2- Concentrations in atomic percent of nitrogen, oxygen, hydrogen, deuterium and hafnium in the samples used in the present work.

Metal	**[N]**	**[O]**	**[H]**	**[D]**	**[^{181}Hf]**
Nb	1.0				0.020
		1.0	1.0		0.065
		0.1		0.2	0.009
Ta	1.1		0.2		0.100
	1.1			1.6	0.087
		0.1	1.2		0.100
		0.1		1.2	0.100

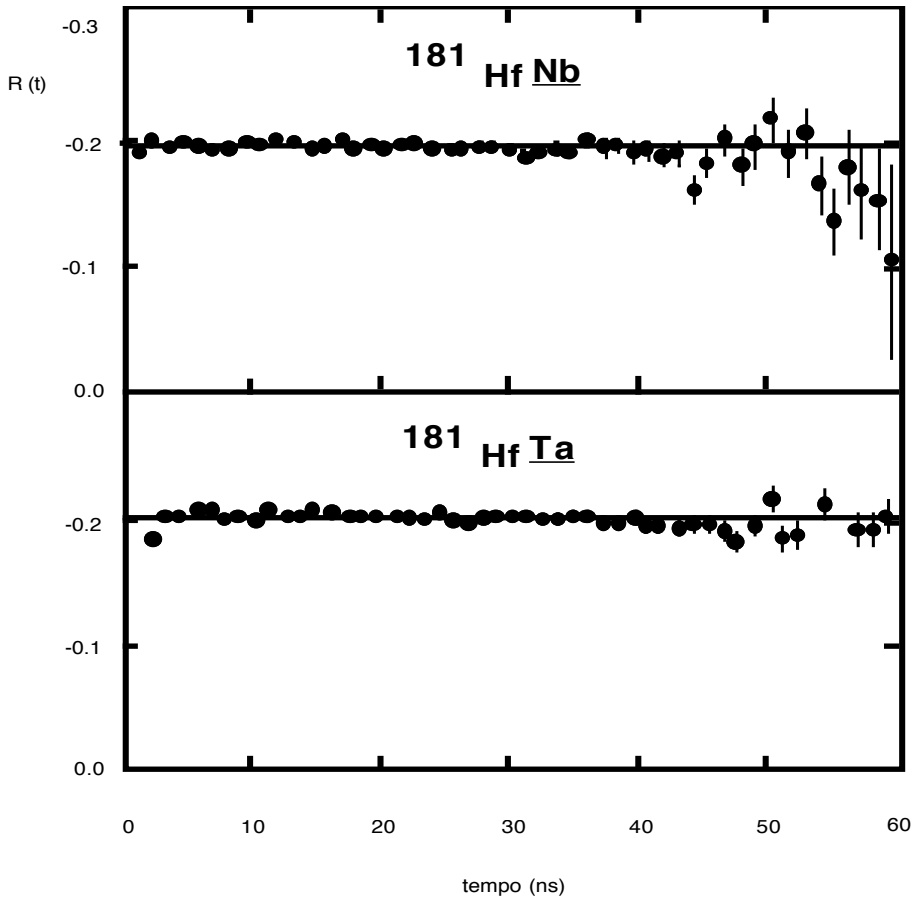

Fig. 3.5- R(t) spectra without perturbation obtained with niobium and tantalum samples after melting with radioactive hafnium.

($P<10^{-7}$Pa). The samples obtained were approximately spherical with 2mm diameter and with around 50mg mass. The hafnium concentrations of the different samples used are indicated in Tab.3.2. After melting the samples are kept at a temperature close to the melting point during 5 to 10 min to eliminate impurities especially oxygen.

As a test for the sample quality a measurement of the perturbed angular correlation is made after melting. If the probe atoms are located in a non-perturbed cubic environment the electric field gradient at the nucleus must be zero and the R(t) curves (see section 3.2) shouldn't present oscillations (Fig.3.5). This confirms the substitutional position occupied by the hafnium

atoms, the absence of impurities after melting and also shows that the number of hafnium atoms in non-cubic environments, such as grain boundaries, is not detectable.

3.2.2 - Nitrogen and oxygen dilution

The dilution of nitrogen or oxygen in the samples is made from the gas phase. Before loading with any of these gases the superficial oxide layer is removed by heating as described before. The pressures and temperatures used are taken from the solubility data for these metals available in the literature [Taylor 67, Smithels 67 e Schulze 77,79]. In the case of tantalum the dilution of oxygen was performed at a temperature of 2300K and a partial pressure of oxygen of $3x10^{-4}$Pa and for nitrogen 2020K and 0.1Pa were used. For niobium the temperatures and pressures used were 2400K and 0.01Pa (or 0.001Pa) for oxygen and 2300K and 0.5Pa for nitrogen.

Special care must be taken to dilute nitrogen in these metals to avoid contamination in particular from oxygen. Indeed the solubility of nitrogen in these metals is much smaller than that of oxygen and oxygen also diffuses faster than nitrogen [Fromm80]. For this reason the initial vacuum before loading was better than $5x10^{-8}$Pa and high purity nitrogen (99.999%) flowed through an adsorbing coal filter in order to eliminate any oxygen impurity. The nitrogen and oxygen concentrations of the samples used are indicated in Tab.3.2.

3.2.3 - Hydrogen and deuterium dilution

Implantation could not be used to dilute hydrogen or deuterium due to the small dimensions of the samples and to the fact that the energies available were too high and would cause unwanted defects during implantation. Dilution from the gas phase was also not used since at the temperatures at which the samples must be heated (of the order of 400°C to 500°C for low concentrations of the order of 1%[Fromm 80]) oxygen from the surface oxide layer diffuses and is captured by hafnium.

The method used was electrolysis in a solution of H_2SO_4 1 molar (for deuterium D_2SO_4 in D_2O was used). The sample is placed in a gold gasket which also makes the electric contact with the rest of the circuit. The electrolytic solution is kept at 80°C for tantalum and 90°C for niobium. At lower temperatures ordered phases of the metal-hydrogen system are formed during electrolysis which may produce small cracks in the sample preventing the control of the hydrogen quantity dissolved. As for deuterium the surface potential barrier is larger than for hydrogen the surface oxide layer is removed before electrolysis. For this purpose the samples are kept for 10 to 15 seconds in an etching solution made from 1ml HNO_3 + 2.5ml of H_2SO_4 (for deuterium D_2O and D_2SO_4 are used) to which 1ml of HF is added immediately before using.

3.2.4 - Hydrogen and deuterium concentration determination

In the electrolysis the concentrations of hydrogen (deuterium) is conditioned by parameters such as the current used, the geometrical shape of the sample, time, temperature, etc. For low concentrations it is possible to pre-

dict empirically the concentration obtained. The exact determination of the concentration is made “à posteriori” after the experiments by vacuum extraction with the vacuum system represented in Fig.3.6.

The samples are heated at 700°C in the oven F, the hydrogen is collected in the reference volume V (the initial vacuum is better than 10^{-4}Pa). The pressure in V is measured with an absolute pressure meter. The procedure is repeated several times in order to extract all the hydrogen in the sample.

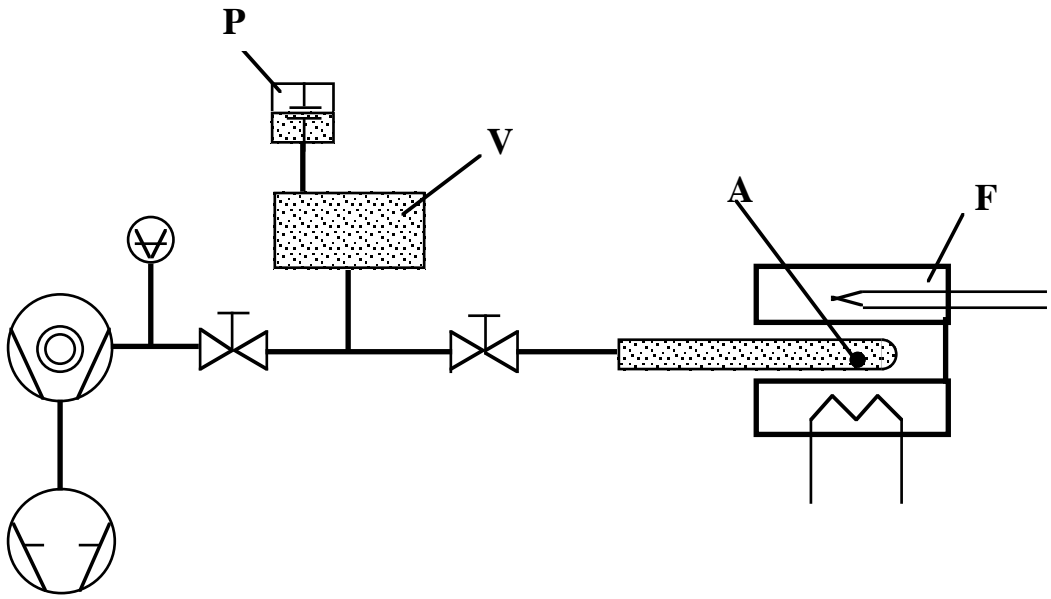

Fig. 3.6 - Vacuum system for hydrogen concentration measurements: *1 and 2 - valves, P - absolute pressure meter, V - reference volume, A - sample and F - oven.*

3.3 - Data analysis

As we refered in chapter 2 in perturbed angular correlation experiments the function $W(\theta,t)$ contains all the information regarding the hyperfine interaction. This function may be obtained experimentally by a convenient analysis of the time spectra. This analysis eliminates the exponential decay and minimizes the effects due to detectors efficiencies, self-absorption in the samples, width and live time of the time analyzer channels, finite time resolution and background coincidences. The most commonly used method for these corrections is based on the use of four detectors and the storage of the different time spectra which are then added in a convenient way as described below.

3.3.1 - The perturbation factor extracted from the time spectra

The coincidence count rate between two detectors i and j, whose axis form an angle θ with a radioactive sample at the vertex is given by

$$C_{ij}(\theta,t) = N_0 \, P_{ij}(\theta,t) \, T_{ij}(t) \, L_{ij}(t) + B_{ij}(\theta,t) \qquad (3.1)$$

where t is the time interval between the detection of γ_1 and γ_2, N_0 is the number of cascades per unit time occurring in the sample, $P_{ij}(\theta,t)$ is the probability of detecting γ_1 and γ_2 at an angle θ with a time difference t, $T_{ij}(t)$ is the live time, $L_{ij}(t)$ is the channel width of the time analyzer and $B_{ij}(\theta,t)$ is the background coincidences count rate.

If we consider a detection system in which the angle θ is defined by two point detectors and the time interval is measured with infinite precision then the probability P_{ij}, for t>0, is given by:

$$P_{ij}(\theta,t) = \frac{1}{\tau_N} e_i\ e_j\ a_{ij}\ e^{-t/\tau_N}\ W(\theta,t) \qquad (3.2)$$

where τ_N is the lifetime of the intermediate state, e_i and e_j are the detector efficiencies of the detectors for the energies of γ_1 and γ_2, a_{ij} is a correction factor due to the source self-absorption and $W(\theta,t)$ is the correlation function of the γ cascade. However the time resolution and the solid angle defined by the detectors are finite and the probability P_{ij} must be corrected accordingly. For $t>\Gamma_t$ (Γ_t is the half maximum width of the time resolution function of the experimental system) the effect of the finite time resolution may be written as an attenuation factor, frequency dependent, which affects the modulation amplitudes of $W(\theta,t)$ [Pleiter 73]. For cylindrical detectors with their axes oriented towards the source the effect of finite solid angle is described by an attenuation factor of each term of $W(\theta,t)$ and which are tabulated [Yates 65]. The correction due to the finite time resolution used is described in section 3.3.2 and no correction due to the finite solid angle was considered as the fits were always normalized to the anisotropy coefficient s_{k0} observed experimentally.

The first step in the manipulation of the experimental data is the subtraction of the background coincidences count rate. The most direct method is to calculate this count rate in a zone of the time spectra where the first term of (3.1) is zero. This occurs for t<0 or $t >> \tau_N$. The live time $T_{ij}(t)$ may influence the background and for high count rates $T_{ij}(t)$ may vary strongly with t. Therefore it is important to subtract correctly the background count

rate since a difference of a few percent in this value may lead to distortions of $W(\theta,t)$ which may be interpreted as hyperfine interactions [Arends 80]. To minimize the effects of $T_{ij}(t)$ low count rates were used and as a sufficient number of channels were available in the multichannel analyzer the background count rate for $t>0$ was always calculated from channels in the region $t>>\tau_N$. With the count rates and counting times used after 5 or 6 τ_N periods there was no appreciable contribution from the decay of the intermediate state.

The count rate corrected for the background $C^+_{ij}(\theta,t)$ is given by:

$$C^+_{ij}(\theta,t) = C_{ij}(\theta,t) - B_{ij}(\theta,t) = N_0 \frac{1}{\tau_N} E_{ij}(t)\, e^{-t/\tau_N}\, W(\theta,t) \qquad (3.3)$$

where $E_{ij}(t) = e_i\ e_j\ a_{ij}\ T_{ij}(t)\ L_{ij}(t)$.

After this operation the zeros of the several spectra must be made to coincide. This is required in order to be able to use the channels for times $t<\tau_N$ [Arends 80]. the time $t=0$ is ideally defined by the centroid of the prompt curve obtained with radiation of the same energies of the γ rays of the cascade. As usually there are no prompt cascades available with the required energies the positron annihilation radiation (obtained for instance from the decay of ^{22}Na) or the prompt cascade of ^{60}Co are used. However in our case the time zero of each spectra were always adjusted before each measurement so that the difference between them is smaller than one or two channels, and therefore the prompt curve was not measured. As long as the difference between the time zero of the several spectra is smaller than the time resolution of the experimental system the misalignment only affects the channels for $t<\tau_N$. Furthermore this effect is partially canceled in the data analysis programme where a first approximation for the time zero

of each spectrum is determined and all spectra are aligned by the same time zero.

With four detectors, and storing the spectra corresponding to the detector combinations of Tab.3.1, to extract the perturbation function from the corrected spectra it is convenient to form the following ratio:

$$R(t) = \frac{2}{3}\left[\left(\frac{C^{+}_{13}(180,t)\ C^{+}_{24}(180,t)}{C^{+}_{14}(90,t)\ C^{+}_{23}(90,t)}\right)^{-\frac{1}{2}} - 1\right] \tag{3.4}$$

by replacing $C^{+}_{ij}(\theta,t)$ in (3.4) we get:

$$R(t) = \frac{2}{3}\left(\frac{W(180,t)}{W(90,t)}\ \delta(t) - 1\right) \tag{3.5}$$

with

$$\delta(t) = \sqrt{\frac{E_{13}(t)\ E_{24}(t)}{E_{14}(t)\ E_{23}(t)}} = \sqrt{\frac{a_{13}\,T_{13}(t)\,L_{13}(t)\ a_{24}\,T_{24}(t)\,L_{24}(t)}{a_{14}\,T_{14}(t)\,L_{14}(t)\ a_{23}\,T_{23}(t)\,L_{23}(t)}} \tag{3.6}$$

From the value of $\delta(t)$ we see that the efficiencies e_i of the different detectors vanish. However in order for $\delta(t)$ to be close to one it is necessary that a_{ij}, $T_{ij}(t)$ and $L_{ij}(t)$ are approximately equal, in first order, for the different detector combinations.

Self-absorption in the sample is important only for thick samples. Numerical studies [Phillips 79] indicate that the coefficients a_{ij} are approximately one for the spherical sources used in this work.

$L_{ij}(t)$ and $T_{ij}(t)$ depend mainly on the electronic system used and on the experimental conditions of the measurements. As their dependence on the delay time t is usually small they are considered to be approximately constant. They may however affect considerably the results if there is a high differential or integral non-linearity of the time to amplitude converter or of the multichannel analyzer. The influence of the experimental conditions was minimized in this work using symmetric geometries, low count rates and similar coincidence count rates in the various detector combinations.

We may then write:

$$R(t) \approx \frac{2}{3}\left(\frac{W(180,t)}{W(90,t)} - 1\right) \qquad (3.7)$$

As was seen in section 2.4 $W(\theta,t)$ for ^{181}Ta may be written as:

$$W(\theta,t) = 1 + A_{22} G_{22}(t)\ P_2(\cos(\theta)) \qquad (3.8).$$

It may be easily seen that, with the approximation $A_{22}G_{22}(t)/2 << 1$, R(t) is given by:

$$R(t) \cong A_{22} G_{22}(t) \qquad (3.9).$$

R(t) is proportional to the perturbation function $G_{22}(t)$ which contains all the information regarding the hyperfine interaction between the nuclear moment and the crystalline fields. The analysis of the data in order to obtain the interaction parameters is made from (3.9).

3.3.2 - R(t) fitting

The perturbation factor for the probe atom used with an axial symmetric electric field gradient and a policrystalline sample may be written as (see section 2.4):

$$G_{22}(t) = \sum_{n=0}^{3} s_{2n} \cos(n \omega_0 t) \qquad (3.10).$$

Often the electric field gradient is not the same for all the nuclei of the observed ensemble but presents a distribution around a mean value. As a consequence of this field gradient distribution the modulation amplitudes s_{2n} are affected by a frequency dependent factor [Forker 73]. For low defect concentrations and moderate temperatures this field gradient distribution may be approximated by a lorentzian distribution with width σ. The perturbation factor is then given by:

$$G_{22}(t) = \sum_{n=0}^{3} s_{2n} e^{-n\sigma t} \cos(n \omega_0 t) \qquad (3.11).$$

The attenuation of the modulation amplitudes due to the finite time resolution of the experimental system is more important when $\omega_0 \Gamma_t > 2\pi$. In these conditions, if we admit that the resolution function is a gaussian with width σ_t ($\sigma_t = \Gamma_t / 2.35$) we may write [Pleiter 73]:

$$G_{22}(t) = \sum_{n=0}^{3} s_{2n} e^{-n\sigma t} e^{-\frac{1}{2}(n\omega_0 t/\sigma_t)^2} \cos(n \omega_0 t) \qquad (3.12).$$

When in the same sample there are k different electric field gradients the perturbation factor may be written as follows:

$$G_{22}(t) = f_0 \sum_{n=0}^{3} s_{2n}\, e^{-n\sigma_0 t} + \sum_{i=1}^{k} f_i \sum_{n=0}^{3} s_{2n}\, e^{-n\sigma_i t}\, e^{-\frac{1}{2}(n\omega_{0i}t/\sigma_t)^2} \cos(n\,\omega_{0i}\,t) \qquad (3.13)$$

where f_i (i=1,...,k) are the fractions of probe atoms perturbed by the electric field gradient i and f_0 is the fraction of probe atoms unperturbed or perturbed by a distribution of electric field gradients close to zero.

In the general case of field gradients without axial symmetry ($\eta \neq 0$) the amplitudes s_{2n} are functions of η and the transition frequencies are no longer integer multiples of the lowest frequency ω_0. The perturbation factor is then given by:

$$G_{22}(t) = f_0 \sum_{n=0}^{3} s_{2n}\, e^{-n\sigma_0 t} + \sum_{i=1}^{k} f_i \sum_{n=0}^{3} s_{2n}(\eta_i)\, e^{-n_n(\eta_i)\sigma_i t}\, e^{-\frac{1}{2}(n_n(\eta_i)\omega_{0i}t/\sigma_t)^2} \cos(n_n(\eta_i)\,\omega_{0i}\,t) \qquad (3.14)$$

with $s_{2n}(\eta)$ and $n_n(\eta)$ ($n_n(\eta=0)=n$) different for each interaction and functions of η. The experimental curve R(t) is adjusted to the function $A_{22}G_{22}(t)$ with $G_{22}(t)$ given by (3.14) by the least squares method using a gradient algorithm [Bevington 69]. The adjustable parameters for each interaction are : the fraction of atoms influenced by the interaction f_i, the frequency ω_{0i} (proportional to the electric field gradient), and the width of the electric field gradient distribution σ_i around ω_{0i}. The statistical error is calculated according to the theory of the propagation of errors for this algorithm [Bevington 69]. In the analysis programme used the fit of the parameter η is not included. The values presented for this parameter were obtained calculating the minimum of χ^2 by varying systematically the value of η. The error

in η was calculated by the usual approximation of the quadratic variation of χ^2 with η around the minimum [Bevington 69].

3.3.3 - The Fourier transform

The determination of an approximate Fourier transform from the experimental curve R(t) is often useful for the initial choice of the fitting parameters. This selection of initial parameters is further simplified by comparing the Fourier spectrum with a Fourier sinthesys generated with those values.

Algorithms for Fourier analysis of functions whose analytical representation is unknown and are described by a table of N discrete values known as Fast Fourier Transforms (FFT) were developed (see for instance [Brigham 82]). These algorithms generate a Fourier spectra also as a table of discrete values.

As can be seen from the expression of $G_{22}(t)$ for each different quadrupole interaction three frequencies appear in the Fourier spectra. The amplitudes of these frequencies in the Fourier spectra are proportional to the s_{2n} coefficients and form the "signature" of the interaction (see for instance the Fourier spectra of Fig.4.1) which allows the easy distinction of the different interactions present.

With the analysis programme used we may calculate the Fourier spectra either from the experimental curve R(t) or from the theoretical curve calculated with the adjusted parameters. The comparison of these two Fourier transforms is a further confirmation of the goodness of the fits.

CHAPTER 4

OXYGEN AND NITROGEN STUDIES IN TANTALUM AND NIOBIUM

As oxygen and nitrogen present a high solubility in the metals of the Vb group of the periodic table, vanadium, niobium and tantalum, studies with high concentrations of these elements may be performed without perturbations due to precipitates. However internal friction studies in these systems suggest the formation of O_n complexes in these metals due to precipitation for concentrations as low as 1 at.% [Cost 84]. On the other hand results in high purity systems suggest a repulsive interaction between oxygen atoms [Weller 85b] which should inhibit the formation of the complexes suggested by Cost. A similar behaviour should be observed for nitrogen. Weller and Giballa [Weller 85a, Gibala 85] suggest that the complexes observed are due to the interaction of oxygen with nitrogen which exists as an impurity in the samples. Inelastic X-Ray studies [Schubert 84, Dosch 85] confirm the non-existence of nitrogen precipitates in niobium.

4.1 - Experimental results

The study of the quadrupole interaction due to hydrogen (deuterium) trapped at oxygen (nitrogen) requires a previous knowledge of the interac-

tions due to oxygen and nitrogen alone as well as the temperature dependence of the parameters characterizing these interactions. These experiments were done with the samples indicated in Tab.3.2 before loading with hydrogen or deuterium. The samples were placed in a closed cycle helium criostat and the system described in section 3.1 was used for the measurements.

4.1.1 - The Ta-O system

The interaction due to oxygen in tantalum is already known [Weidinger 81]. In the present work the same interaction with parameters ν_Q=597MHz and η=0.35 at 10K was observed (Tab.4.1). The experimental R(t) spectra as well as it's Fourier spectra are represented in Fig.4.1. In Fig.4.2 the temperature dependence of ν_Q and η is shown. From this figure we may see that the interaction frequency decreases with increasing temperature while the asymmetry parameter increases in the same range.

Tab. 4.1- Interaction frequencies ν_Q and asymmetry parameters η of the interactions due to oxygen and nitrogen impurities and to their complexes with hydrogen and deuterium in niobium and tantalum at 10K.

	N	**NH**	**ND**	**O**	**OH**	**OD**
Nb	495(2) 0.28(1)	—	—	275(1) 0.57(1)	208(1) 0.48(2)	207(3) 0.48(2)
Ta	192(1) 0.50(2)	240(3) 0.80	250(2) 0.80	597(1) 0.35(1)	585(1) 0.72(1)	580(3) 0.68(2)

4.1.2 - The Ta-N system

Only one interaction is observed in this system after loading with nitrogen. This interaction is characterized by ν_Q=192MHz and η=0.50 (Tab.4.1). As for the previous system R(t) and Fourier spectra at room temperature are presented in Fig.4.1 and the temperature dependence of the interaction parameters is in Fig.4.2.

Although only two experiments were performed, at 8K and 300K, it can be seen that ν_Q increases with temperature. The big error bars in the experimental values for η do not allow any conclusions to be made about this parameter's temperature dependence.

4.1.3 - The Nb-O system

In this system only one well defined interaction is observed characterized by an interaction frequency ν_Q=275MHz and η=0.57 (Tab.4.1). The temperature dependence of these parameters is shown in Fig.4.2 and typical R(t) and Fourier spectra for room temperature are shown in Fig.4.1.

The interaction frequency depends weakly on temperature below 250K while the η parameter increases significantly in the same temperature range.

4.1.4 - The Nb-N system

This was the only system where more than one interaction could be adjusted to the experimental spectra. Besides the interaction ν_{Q1}=495MHz and

η_1=0.28 presented in Tab.4.1, two other interactions with smaller fractions are observed characterized by ν_{Q2}=240MHz and η_2=0.68 and ν_{Q3}=350MHz and η_3=0.73. The R(t) and Fourier spectra are shown in Fig.4.1. The interaction ν_{Q1} indicated by the lines in the Fourier spectrum is clearly dominant over the other two. In two different samples which were loaded with nitrogen in the same conditions and with similar concentrations (see Tab.3.2) it was observed that in each sample the fraction of probe atoms perturbed by ν_{Q2} and ν_{Q3} is smaller than the fraction of ν_{Q1} and the ratio of these three fractions is constant with temperature. However this ratio depends on the sample considered. The ratio (f_1: f_2: f_3) of the observed fractions was (1 : 0.6 : 0.3) and (1 : 0.3 : 0.5) for the two samples studied. On the other hand while ν_{Q1} and η_1 are identical between the two samples ν_{Q2}, η_2 and ν_{Q3}, η_3 vary by approximately 16% in the same samples. Within the experimental uncertainty no significant variation of these parameters with temperature was observed.

These facts lead to the conclusion that the interactions ν_{Q2} and ν_{Q3} must be due to a mixture of different complexes, which are stable in the temperature range studied, and that the number of these defects depend strongly on the conditions in which samples are prepared. The well defined and sample independent interaction ν_{Q1} must be due to the interaction of one single nitrogen atom with the hafnium probe.

The temperature dependence of ν_{Q1} and η_1 is shown in Fig.4.2. We may see from this figure that ν_{Q1} is almost constant while η_1 is constant up to 150K and then increases slightly.

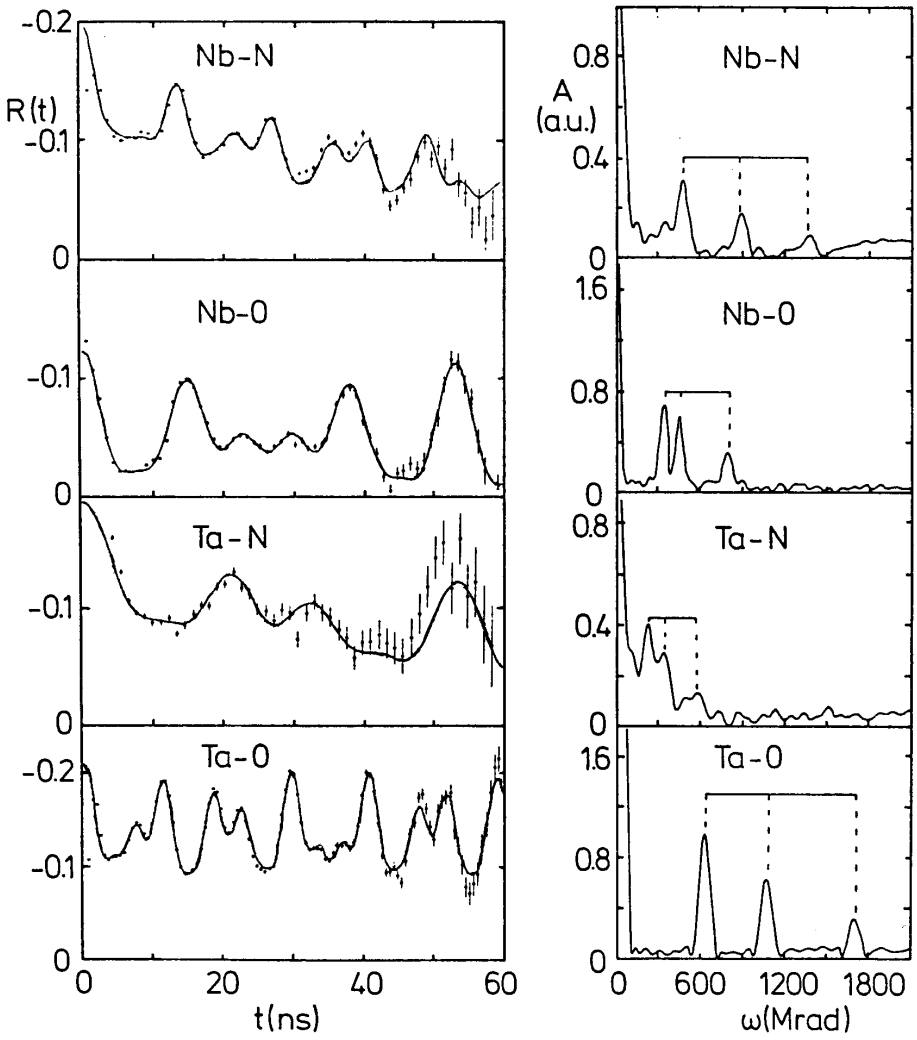

Fig. 4.1- a) R(t) spectra at 300K of niobium and tantalum samples loaded with nitrogen and oxygen. The full lines are fits of (3.14) to the experimental data.

b) Fourier spectra of the same data. In each spectra the transition frequencies for the interaction observed (Tab.4.1) are indicated by dashed lines.

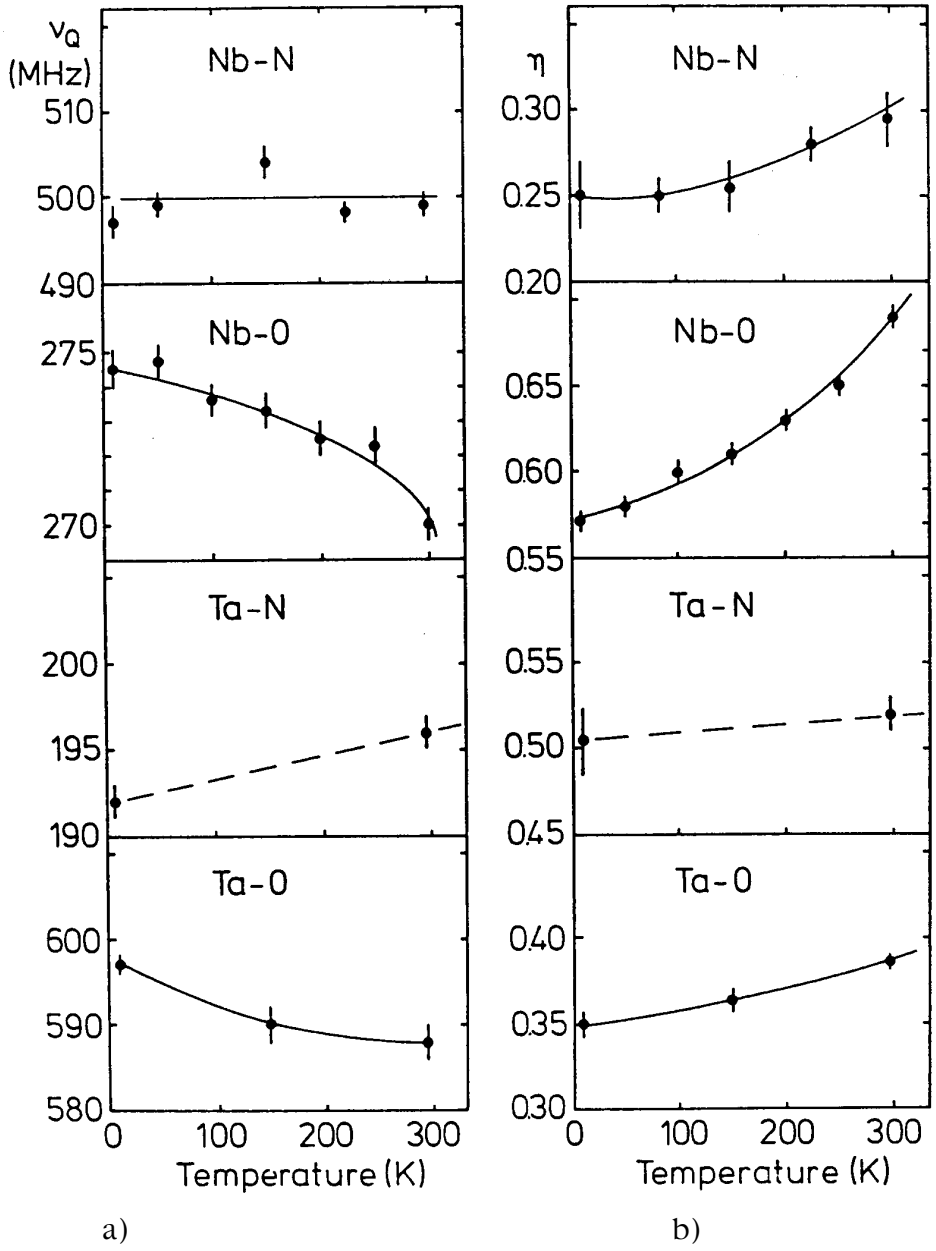

Fig. 4.2- a) Temperature dependence of the interaction frequency and, b) of the asymmetry parameter for the interactions due to nitrogen and oxygen in niobium and tantalum. The full lines do not correspond to fits but are merely to guide the eye.

4.2 - Discussion

In order to understand the relative values of the interaction parameters for the different systems, information about the position of the probe atom relative to the interstitial impurity is required. The position occupied by oxygen and nitrogen in the metallic lattices of niobium, tantalum and vanadium has been determined by ion channeling experiments [Hiraga 77, Takahashi 78, Kaim 79, Carstanjen 82, Shakun 85] which have shown that both oxygen and nitrogen occupy interstitial octahedral positions in these metals. By performing perturbed angular correlations in single crystals Wrede et all [Wrede 86] concluded that in order to justify the orientation of the observed electric field gradient, oxygen in niobium must occupy the octahedral position which is 2^{nd} nearest neighbour to the probe atom. The positions of oxygen and hafnium in niobium according to these authors is presented in Fig.4.3.

The values of the interaction frequencies and of the asymmetry parameters are presented for comparison in Fig.4.4.

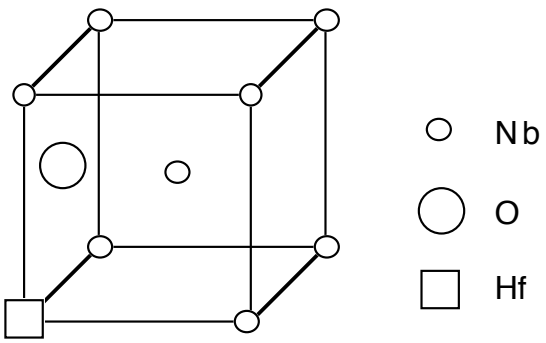

Fig. 4.3 - Cubic unit cell showing the positions of oxygen and of ^{181}Hf in niobium according to Wrede et all [Wrede 86]. Oxygen is 2^{nd} nearest neighbour to hafnium.

4.2.1 - The interaction frequencies ν_Q

Due to their low diffusion coefficient in the temperature range studied oxygen and nitrogen when captured by hafnium remain immobile in their interstitial positions after the decay of the probe atom. On the other hand as the first excited state of the ^{181}Ta cascade has a lifetime of 25.7μs (Fig.2.3) and as the electronic relaxation times in metals are of the order of picoseconds and the lattice ion relaxation times are of the order of nano-seconds, when the angular correlation is observed there is no longer any influence of the original charge distribution due to the probe atom ^{181}Hf. Therefore we may consider that the system studied consists of the metallic lattice, the radioactive atom ^{181}Ta and the oxygen or nitrogen impurity.

If the positions of oxygen and nitrogen relative to the radioactive atom are the same, the variation of the interaction frequencies must be essentially due to differences of the electronic charge distribution caused by the different valence of oxygen and nitrogen and, in the case of niobium, also due to the radioactive atom which is an impurity in this metal.

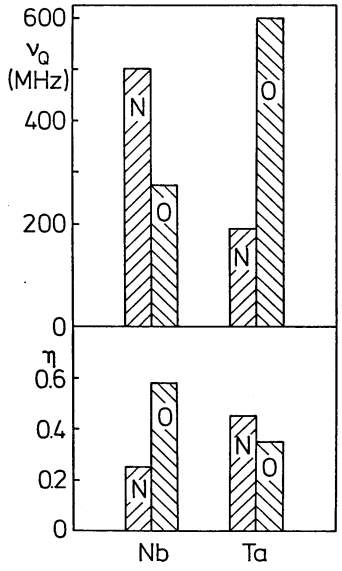

Fig. 4.4- Bar chart with the interaction parameters for oxygen and nitrogen in niobium and tantalum.

Therefore as the electronegativity of tantalum is smaller than that of niobium the radioactive atom in this metal will polarize the bonding orbitals of the impurity increasing the electronic density in it's vicinity. This effect

will be stronger for nitrogen since this atom may receive up to three electrons in it's valence shell as opposed to two in oxygen. For this reason we expect that the interaction frequency due to nitrogen is larger than that due to oxygen in this metal, $\nu_{QN} > \nu_{QO}$, and that is what was experimentally observed (see Fig.4.4).

In tantalum the charges involved are the same but as the radioactive atom is the same as the lattice atoms, this charge will be equally distributed by all the nearest neighbours of the interstitial impurity. As the bonding orbitals of oxygen and nitrogen are p orbitals the distribution of charge is larger for nitrogen, since it may receive three electrons which are then distributed by it's 6 nearest neighbours, than for oxygen where the electrons received form bonds to the four 2^{nd} nearest neighbours avoiding the high electronic density of the 1st nearest neighbour tantalum atoms. Therefore in spite of nitrogen attracting more electrons we expect oxygen to give rise to a higher interaction frequency, $\nu_{QN} < \nu_{QO}$ as was experimentally observed (see Fig.4.4).

The observation of more than one interaction frequency in the Nb-N system shows, as was already mentioned, that several types of defects with different numbers of nitrogen atoms are captured by the hafnium probe. The formation of these precipitates seem to be strongly dependent on the sample preparation particularly the cooling procedure. Cooling of samples by flowing cool helium into the vacuum chamber immediately after switching the heating current off has been successfully used to quench the high temperature α phase random distribution of nitrogen atoms in niobium and no precipitates have been observed [Rowe 80, Schubert 84]. The samples used in the present work were cooled simply by switching the electron gun current off. The electron gun is enclosed in a glass enclosure with only one open end in order to prevent the radioactive contamination of the vacuum

chamber. This difficults the gas flow around the sample and we should expect to have low cooling rates in this conditions. In the samples studied an equal number of probe atoms with only one nitrogen and with more than one nitrogen atom in it's vicinity are observed which indicates that the number of nitrogen atoms in precipitates is high. This indicates that substitutional hafnium is an efficient trapping center for nitrogen as, according to the phase-diagram for this system, at room temperature and for 1 at.% nitrogen in niobium only approximately 5% of the nitrogen atoms precipitate. With the results available the identification of the complexes causing the two extra interactions is not possible.

4.2.2 - The asymmetry parameters η

An increase of the asymmetry parameter when the temperature is increased from 10K to 300K is observed for all systems. The relative variation of this parameter is larger for niobium than for tantalum, while in tantalum this variation is smaller than 10% in niobium is approximately 20% in the same temperature range. This larger variation of η in niobium may be due to an additional distortion of the electronic charge distribution due to the fact that the radioactive atom (^{181}Ta) is an impurity in this lattice.

From the definition of the asymmetry parameter, $\eta = (V_{yy} - V_{xx})/V_{zz}$, we may see that a larger value of η corresponds to a charge distribution which is more compressed into a plane. Thus we may understand more easily the η values for oxygen and nitrogen in niobium where the bonding electrons are more attracted towards the radioactive atom. The two oxygen electrons will occupy p bonding orbitals and are localized preferentially in the (100) plane which contains the interstitial impurity creating a low symmetry

charge distribution and therefore a high η. The three bonding electrons in nitrogen are not able to concentrate in the (100) plane due to the orthogonality of the p orbitals. Therefore the charge density outside this plane is increased and the value of η decreases.

Wrede [Wrede 86] used a point charge model in order to justify the asymmetry parameter observed in the Nb-O system. In this model a covalent contribution to the bonding of oxygen to tantalum is considered The oxygen bonding p electrons occupy orbitals at an angle of 90°, this situation is simulated with two additional charges in the (100) plane at an equal distance from tantalum and from oxygen but outside the axis joining them as is shown in Fig.4.5a. This configuration is justified by the fact that the electrons will avoid the high electronic density outside this plane. Considering the Pauling electronegativities of oxygen and tantalum [Cotton 66] the bond between these two atoms is approximately 63% ionic and a charge of -1.26e is localized on the oxygen atom and two charges of -0.37e are delocalized. The experimental value of η is thus reproduced with the principal axis of the electric field gradient (V_{ZZ}) in the <100> direction which contains the oxygen atom, if the delocalized charges are moved towards the Ta-O axis. In this model only the bond between the oxygen and tantalum atoms is considered. For the Ta-O system this approximation is no longer valid because the radioactive atom ^{181}Ta is equal to the lattice atoms. If we consider that the p bonds are shared with the four nearest neighbours in the (100) plane (Fig.4.5b), the value of η calculated is 0.31 close to the experimental value of 0.35.

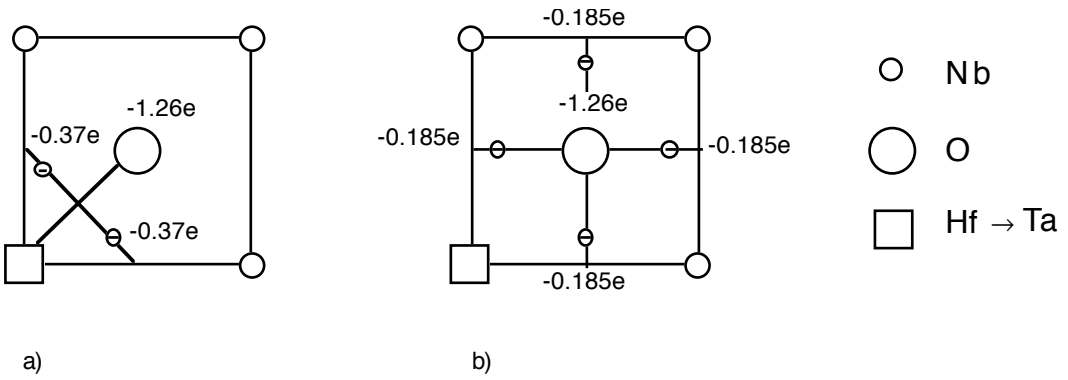

Fig. 4.5 - Positions in the (100) plane of the charges used in the point charge model : a) oxygen in niobium; b) oxygen in tantalum.

The same qualitative argument used to justify the η variation between oxygen and nitrogen in niobium when applied to tantalum leads to conclusions which are in contradiction with the experimental results as in this metal the value of η for nitrogen is larger than for oxygen. The low symmetry responsible for the high η value may be due to the symmetry difference between the interstitial position with octahedral symmetry occupied by nitrogen and the symmetry of the valence shell, either cubic (p orbitals) or tetrahedral (sp^3 hybridization). The possibility that nitrogen occupies the next nearest neighbour octahedral site close to the hafnium must be excluded because as nitrogen is closer to the probe atom a larger interaction frequency than for oxygen would be expected and this is not observed experimentally and furthermore the same symmetry discrepancies exist in this case.

4.2.3 - The temperature dependence of ν_Q and η

The temperature dependence of the values of ν_Q and η may be attributed to small changes of the charge distribution in the vicinity of the radioactive atom. This charge distribution is altered by the increase of the ion oscillations and by the lattice expansion. These contributions are coupled and lead to the well known "$T^{3/2}$ law" for the temperature dependence of the electric field gradient - $V_{zz}(T) = V_{zz}(T=0)(1 - B\ T^{3/2})$ - [Christiansen 76]. However there is no definite trend of this dependence for impurities in cubic metals [Witthuhn 83] which is confirmed by the present results. Fig.4.2 shows that the behaviour of the electric field gradient strength with temperature is different for all the systems studied. In Ta-O the variation curve of ν_Q with temperature has a negative slope and a positive curvature, in Ta-N the slope is positive and in Nb-N is approximately constant. Only in the Nb-O system is both the slope and curvature negative and a fit of the data to the "$T^{3/2}$ law" may be done. However the value of B obtained ($B= 2.7x10^{-6}\ T^{3/2}$) is one order of magnitude lower than the values obtained for non-cubic metals [Vianden 83]. As may be seen from Fig.4.2 the negative slope observed for the variation of ν_Q with temperature for oxygen is not observed for nitrogen. The small relative variation of ν_Q in all systems (smaller than 2%) indicates that the different contributions (thermal oscillations, electronic charge distribution variation and lattice expansion) either are very small or in some way compensate each other. In the latter case small variations in the relative values of these contributions would justify the different behaviours observed.

Regarding the temperature dependence of η this parameter increases in all systems with a larger variation in the case of niobium. Possibly an increase of the interaction between the impurity valence electrons and the

metal electrons may constrain the electronic charge distribution to certain crystal planes decreasing the charge distribution symmetry and causing an increase in the value of η. The fact that the radioactive atom is a defect in niobium may justify the stronger increase of η in this metal.

4.3 - Conclusions

From the perturbed angular correlation experiments made in low concentration alloys of niobium and tantalum with nitrogen and oxygen we may conclude the following:

- The single and well defined interactions observed for oxygen and nitrogen in tantalum and for oxygen in niobium, are due to trapping of one single interstitial impurity atom and no higher order complexes are observed.
- In the Nb-N system the interaction due to one nitrogen atom is observed and also interactions due to complexes of more than one nitrogen atom. The formation of these complexes is strongly dependent on the nitrogen dilution method. In order to avoid the formation of these complexes quenching rates higher than those used for the other systems are needed. The two additional interactions observed in this system suggest the existence of at least two distinct configurations for these complexes although an identification of their structure has not been possible.
- Oxygen in niobium occupies an octahedral interstitial position which is 2^{nd} nearest neighbour to hafnium and the same should hold for tantalum. The present results and the models used do not allow similar conclusions to be made for nitrogen. The location of this atom in both the 1^{st} or 2^{nd} nearest neighbour position relative to hafnium is possible being excluded the simultaneous occupation of both sites as it is hard to

understand why only complexes of two atoms would be formed. On the other hand the occupation of one site or the other is also excluded since that would lead to two different electric field gradients and only one well defined interaction is observed in both metals.

- The temperature dependence of the interaction frequencies is very small and shows no definite trends. The larger variation of η with temperature in niobium is attributed to the fact that ^{181}Ta is an impurity in this metal.
- The relative values of the electric field gradients (proportional to the interaction frequencies) may be understood in terms of the valence electrons of oxygen and nitrogen and of their spatial distribution relative to the probe atom.
- The symmetry of the electric field gradient observed for oxygen in tantalum and niobium may be understood in terms of a simple point charge model involving the valence electrons of oxygen. For nitrogen a decrease of η caused by the higher symmetry of it's valence orbitals is expected and is observed in niobium. The opposite behaviour observed in tantalum is probably due to differences in the impurity valence orbital symmetry relative to it's position in the lattice.

CHAPTER 5

STUDIES OF THE INTERACTION OF HYDROGEN AND DEUTERIUM WITH OXYGEN AND NITROGEN IN TANTALUM AND NIOBIUM

5.1 - Introduction

The trapping of hydrogen and deuterium by interstitial impurities such as oxygen and nitrogen has been extensively studied by several methods. It has generally been accepted that the interaction responsible for the trapping of hydrogen by defects is partly due to the lattice elastic deformations in their vicinity [Shirley 83]. The tetragonal symmetry of the deformation field due to carbon, nitrogen and oxygen in body centered cubic metals is well established [Shirley 83, refs Tab.1]. Quasi-elastic neutron scattering measurements in niobium with deuterium have shown that the deformation field for this impurity has cubic symmetry [Bauer 75]. Using inelastic X-Ray scattering (Huang scattering) Metzger et all [Metzger 76] confirmed the results of Bauer et all showing that the distortion field for hydrogen in niobium also presents cubic symmetry. However Metzger et all [Metzger 85] observed a tetragonal symmetry for the N-H complex in niobium indicating

that the symmetry of the trapping center predominates over that due to hydrogen.

Using electrical resistivity methods Pfeiffer and Wipf [Pfeiffer 76] and Rosan and Wipf [Rosan 76] suggested that the reorientation of the N-H pairs in niobium is short ranged and precipitation is suppressed when the hydrogen concentration is smaller than that of nitrogen. These authors also concluded that only one hydrogen atom is trapped by nitrogen in niobium. This was also observed for oxygen in niobium [Mattas 75 and Sado 82]. Internal friction results showed that the trapped hydrogen position is temperature dependent [Zapp 80a, Hanada 81a and 81b].

The general picture of trapping that emerges from these experimental investigations is that a single hydrogen atom moves around on several interstitial sites (tetrahedral or quasi- tetrahedral) near an immobile impurity atom located at an octahedral site.

The structure of these complexes is still controversial. The first structures suggested by internal friction studies for the complex O-H in niobium [Schiller 75, Zapp 80a] are in contradiction. While Schiller and Nijam suggest a trigonal symmetry for the O-H pair in the <111> direction (considering hydrogen located in octahedral sites), Zapp and Birnbaum propose that hydrogen tunnels between several interstitial positions in rings around the oxygen atom excluding the octahedral positions and the <111> symmetry.

The structure of the N-D pair in tantalum has been studied by channeling Carstanjen 80]. This system is, in principle, similar to N-H in niobium [Rosan 76]. Carstanjen observed that nitrogen is located in an octahedral position in tantalum and remains immobile when trapping a deuterium atom. The trapping sites suggested for deuterium were later revised [Carstanjen 82] but the only safe conclusion was that the deuterium sites are not

located in the same face of the unit cell where the nitrogen impurity is found.

At very low temperatures the N-H system shows an anomalous increase of the specific heat [Morkel 78] attributed to tunneling of hydrogen between two equivalent trapping sites close to nitrogen. This is supported by a neutron diffraction experiment [Wipf 81] where the distance between the two trapping sites was found to be around 0.1Å. In an inelastic neutron scattering study Magerl et all [Magerl 83] found that the local mode vibration energies of hydrogen in niobium are not altered when this is trapped by nitrogen. These authors also conclude that hydrogen remains in tetrahedral positions when trapped but at a sufficiently large distance from the trapping center so that the hydrogen local potential remains practically undisturbed. A N-H distance of 3.5Å was also suggested.

From these results is concluded that in the hydrogen-interstitial impurity complexes configurations in niobium and tantalum hydrogen occupies two neighbour tetrahedral sites tunneling between them. These two sites must be 4^{th} nearest neighbour to the interstitial impurity. At higher temperatures hydrogen diffuses to the other interstitial positions available around the trapping center until it receives enough energy to diffuse away.

5.2 - Experimental results

In the present studies of the interaction between hydrogen or deuterium and nitrogen or oxygen the samples shown in Tab.3.2 were used. All perturbed angular correlation measurements were made with the samples inside the closed cycle helium cryostat and with the experimental system described in chapter 3.

5.2.1 - The Ta-O-H(D) system

After loading Ta-ø samples with hydrogen only the well known oxygen interaction frequency is observed at room temperature. At low temperatures a new interaction frequency is observed with ν_Q=585MHz and η=0.72. This interaction appears at around 55K and as may be seen in Fig.5.1, the fraction of atoms perturbed by this interaction increases rapidly while the fraction of atoms perturbed by oxygen decreases by the same amount when the temperature is lowered [Peichl 83].

When deuterium is added instead of hydrogen a similar behaviour is observed. At room temperature only the oxygen interaction is present and at low temperatures the same interaction as for hydrogen is found. In Fig.5.2 the temperature dependence of the fractions of atoms perturbed by oxygen and by deuterium is presented. Although the behaviour is similar to the previous one the new interaction appears at a higher temperature, 105K, and while for hydrogen the number of oxygen decorated atoms is only 50% for deuterium 75% of the oxygen atoms have a trapped deuterium.

5.2.2 - The Ta-N-H(D) system

In this system at room temperature only the interaction due to nitrogen is observed. At low temperatures two new interactions are observed characterized by ν_{Q1}=240Mhz, η=0.80 and ν_{Q2}=250Mhz, η=0.40. The fractions of probe atoms perturbed by these interactions are approximately equal and disappear simultaneously at around 80K. The nitrogen interaction increases considerably at the same temperature as can be seen in Fig.5.3. As none of

the interactions ν_{Q1} and ν_{Q2} by themselves may justify the variation of the nitrogen fraction we only indicate the sum of these fractions in Fig.5.3.

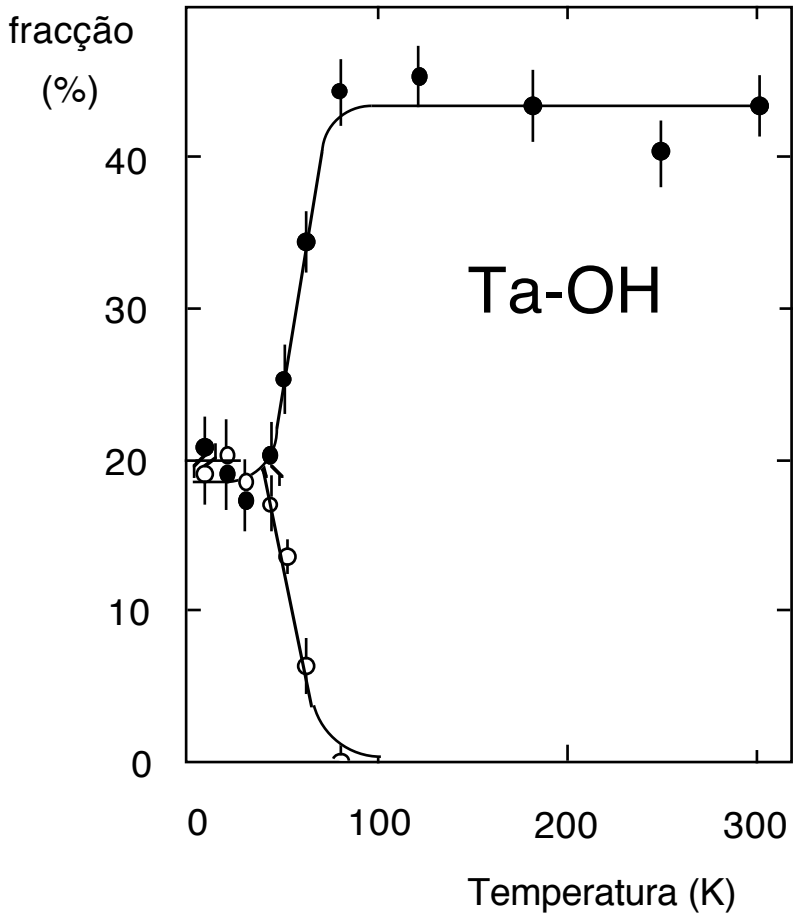

Fig. 5.1- Temperature dependence of the fractions of atoms perturbed by oxygen or an oxygen-hydrogen complex in tantalum. The solid lines are only a guide to the eye.

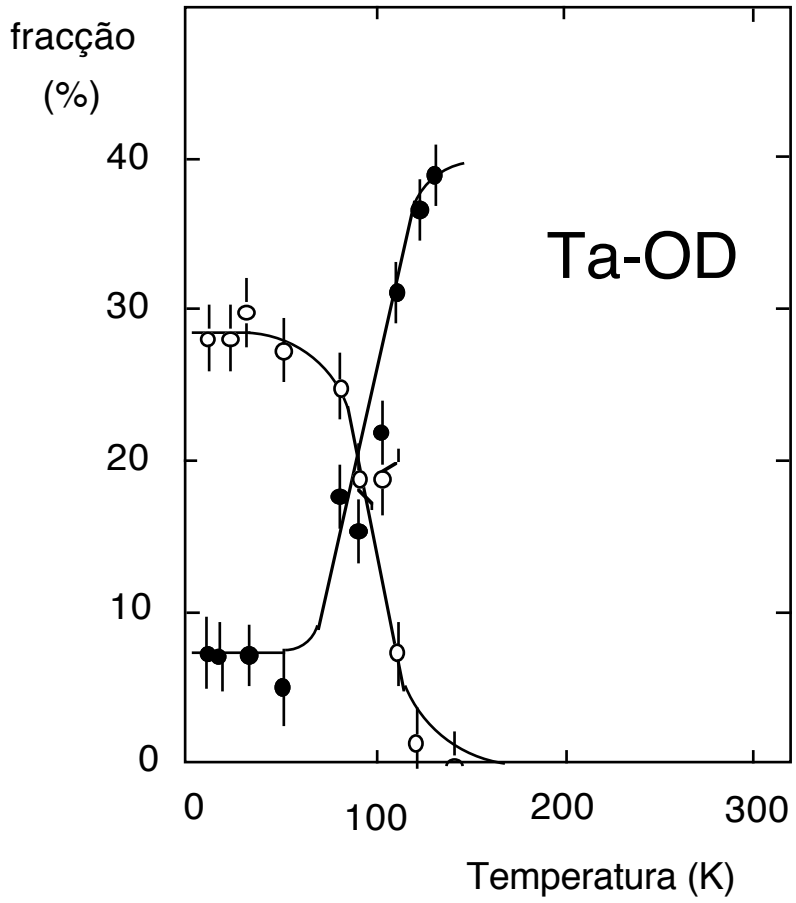

Fig. 5.2- Temperature dependence of the fractions of atoms perturbed by oxygen or an oxygen-deuterium complex in tantalum. The solid lines are only a guide to the eye.

The same interactions are observed when instead of nitrogen deuterium is dissolved in the metal. The fractions of these two interactions are very similar and also disappear at around 110K. In Fig.5.4 the temperature dependence of the sum of these two fractions is shown and in Fig.5.5 the R(t) and Fourier spectra for samples loaded with nitrogen, nitrogen plus hydrogen and nitrogen plus deuterium are shown. It should be noticed that the R(t) spectra for Ta-N-H and for Ta-N-D are similar as well as their Fourier transforms where the interactions observed are indicated.

5.2.3 - The Nb-O-H(D) system

After the dilution of hydrogen in the samples apart from the interaction due to oxygen two new interactions are observed in this metal with ν_{Q1}=208Mhz, η=0.48 and ν_{Q2}=220Mhz, η=0.85. Again the behaviour of deuterium loaded samples is similar and the same interactions are observed [Mendes 85].

The interaction ν_{Q2} is highly stable and it's fraction remains approximately constant in the temperature range from 8K up to room temperature with a value of around 7.5% and 17% for hydrogen and deuterium respectively. In Figs.5.6 and 5.7 the temperature dependence of the fractions of probe atoms perturbed by oxygen and by ν_{Q1} is shown for samples loaded with hydrogen or deuterium. In both cases ν_{Q1} is only observed at temperatures below around 80K .

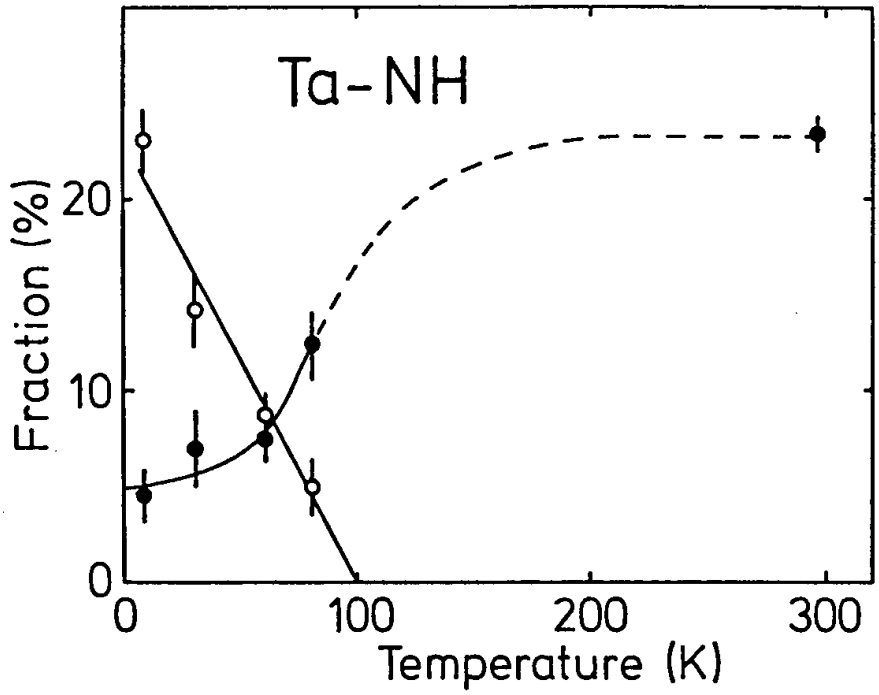

Fig. 5.3 - Temperature dependence of the fractions of atoms perturbed by nitrogen or a nitrogen-hydrogen complex in tantalum. The solid lines are only a guide to the eye.

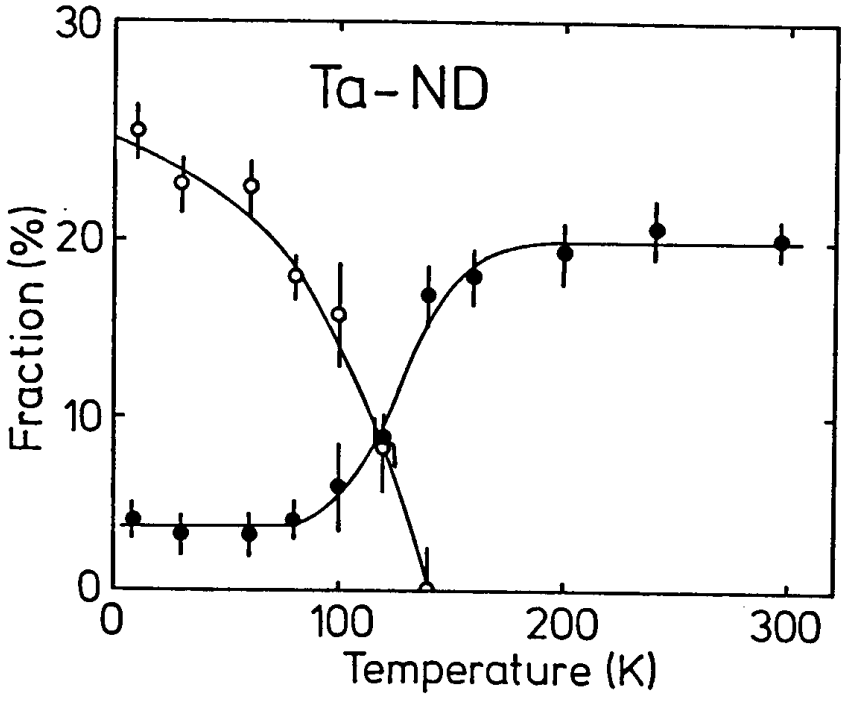

Fig. 5.4 - Temperature dependence of the fractions of atoms perturbed by nitrogen or a nitrogen-deuterium complex in tantalum. The solid lines are only a guide to the eye.

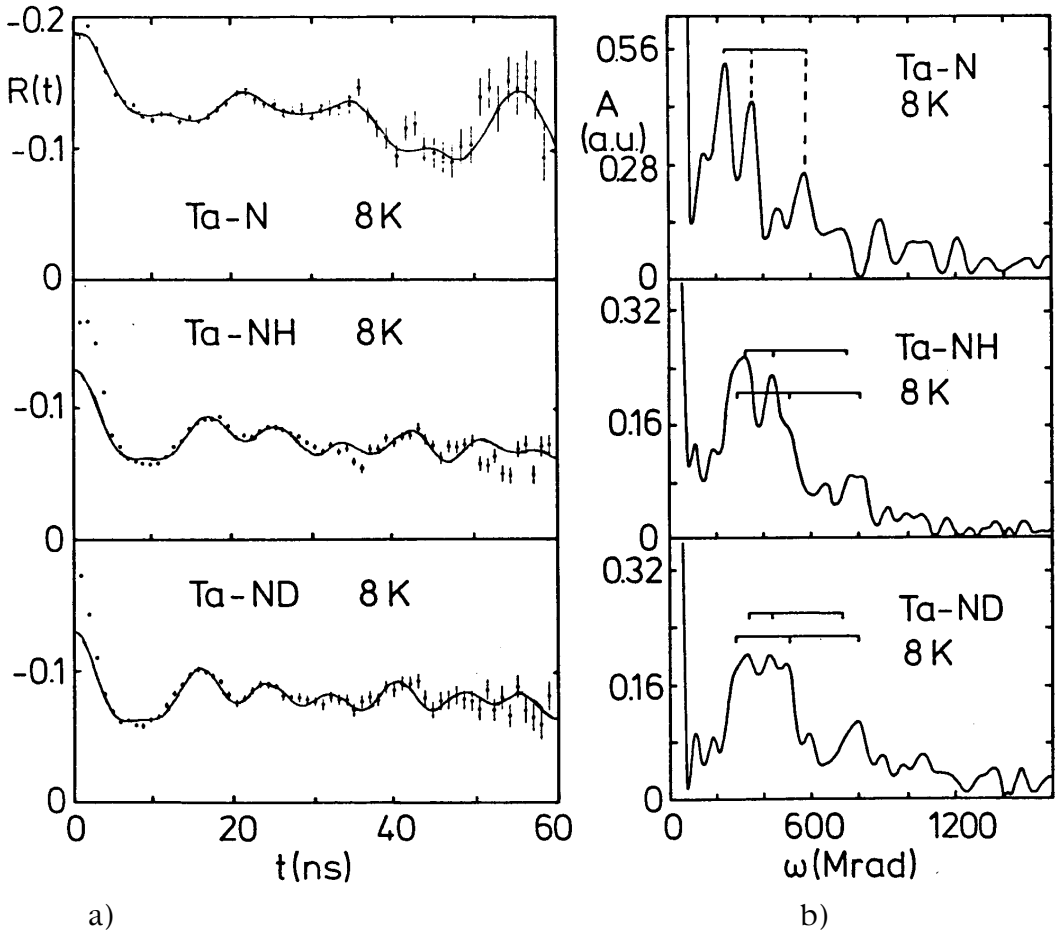

Fig. 5.5 - a) R(t) spectra obtained after loading tantalum with nitrogen and nitrogen plus deuterium, at 8K. The solid lines correspond to fits of (3.14) to the experimental data. b) Their respective Fourier spectra with the three components of the observed interactions indicated by the dashed lines.

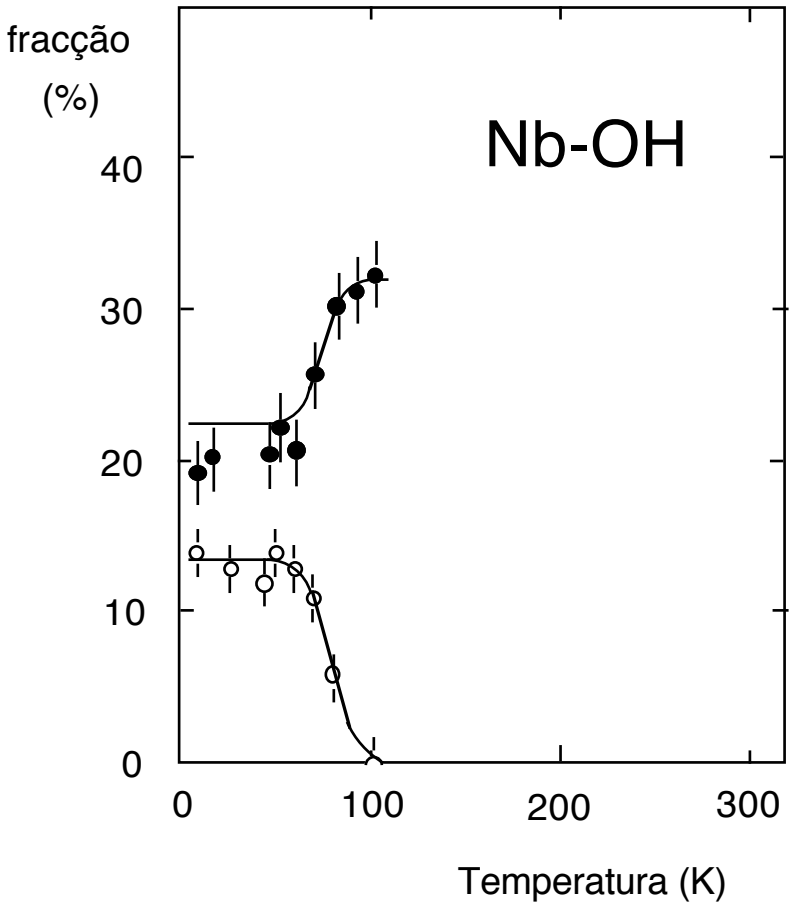

Fig. 5.6 - Temperature dependence of the fractions of atoms perturbed by oxygen or an oxygen-hydrogen complex in niobium. The solid lines are only a guide to the eye.

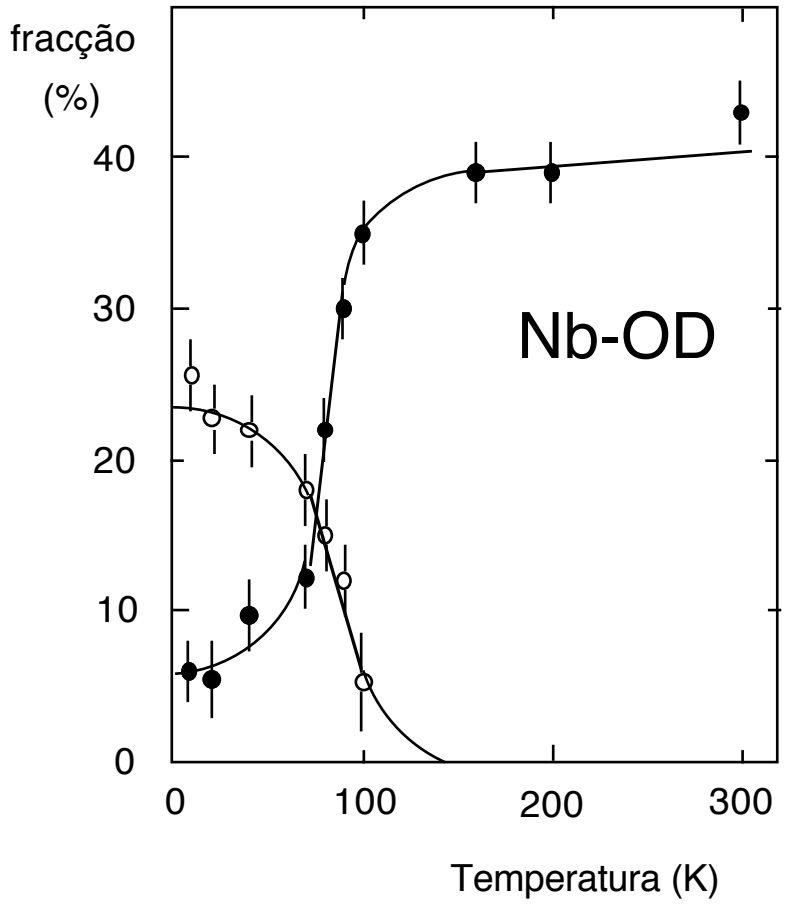

Fig. 5.7 - Temperature dependence of the fractions of atoms perturbed by oxygen or an oxygen-deuterium complex in niobium. The solid lines are only a guide to the eye.

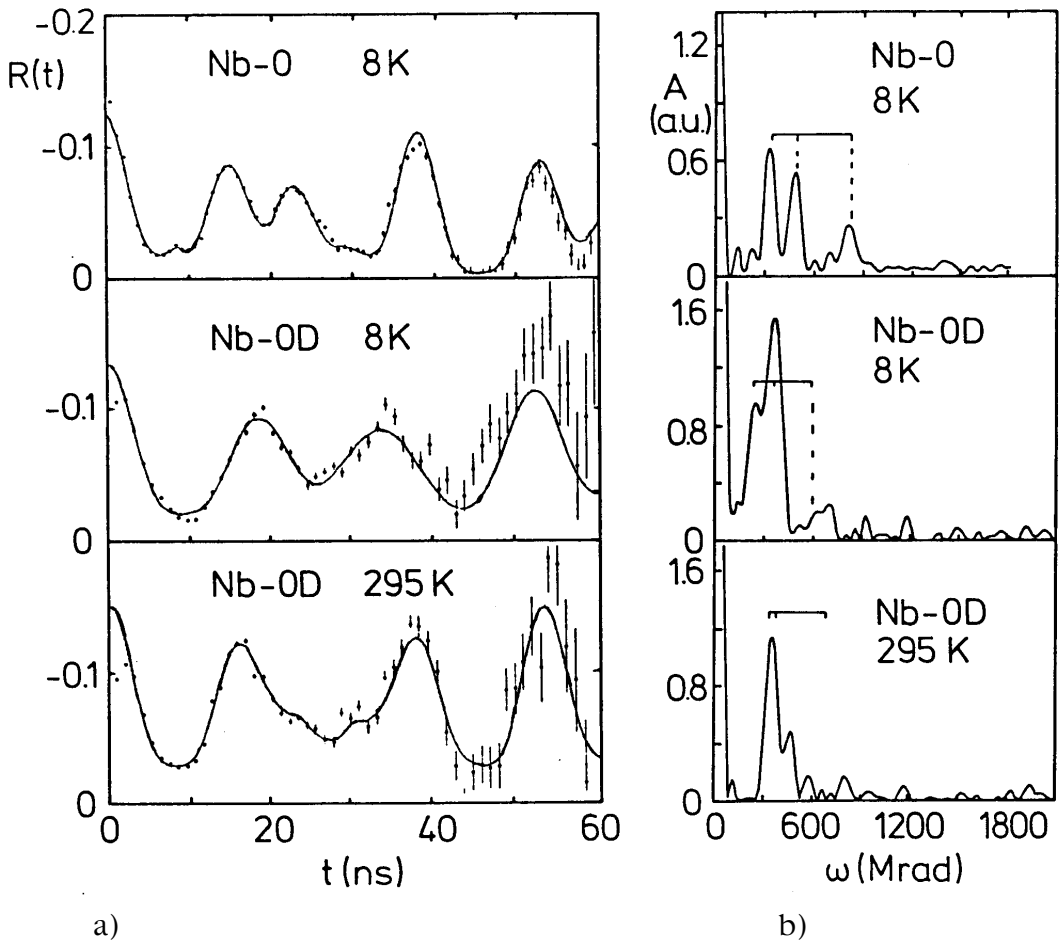

Fig. 5.8 - a) R(t) spectra obtained after loading niobium with oxygen and oxygen plus deuterium, at 8K and 295K. The solid lines correspond to fits of (3.14) to the experimental data. b) Their respective Fourier spectra with the three components of the observed interactions indicated by the dashed lines.

In Fig.5.8 the R(t) spectra and their Fourier transforms after loading a niobium sample successively with oxygen and deuterium is shown. In the absence of deuterium only the oxygen interaction is observed. After loading with deuterium at 295K the interaction ν_{Q2}, indicated in the Fourier spectrum, is also present and at 8K essentially the two interactions ν_{Q1} and ν_{Q2} are observed. In the Fourier spectrum corresponding to the 8K measurement only the low temperature interaction ν_{Q1} is indicated.

5.3 - Discussion

5.3.1 - Assignment of the interaction frequencies ν_Q

As may be seen by the present results in all the systems studied a similar behaviour is observed. There is a large decrease of the fraction of atoms perturbed by the interaction due to oxygen (nitrogen) when the temperature is lowered and simultaneously the number of atoms perturbed by the low temperature interaction increase by the same amount.

The interactions observed with this behaviour are summarized in Tab.4.1. The fact that the low temperature interactions only appear in samples loaded with hydrogen (deuterium) and that they are converted to the oxygen (nitrogen) interaction as the temperature is raised shows that they should be due to trapping of hydrogen (deuterium) atoms by oxygen or nitrogen.

Due to the high hydrogen and deuterium concentrations relatively to oxygen or nitrogen in some of the samples studied (see Tab.3.1) we would expect to see different types of complexes due to trapping of more than one

atom of hydrogen (deuterium). However we only see one well defined interaction with this behaviour. Furthermore the trapping process is reversible since the same transition temperatures and the same behaviour for the fractions are observed when the same sample is submitted to several measurement cycles wether increasing the temperature from 8K to 300K wether decreasing it. These facts show that the new interactions are due to trapping of only one hydrogen (deuterium) atom in the vicinity of oxygen or nitrogen.

As was mentioned before in the Nb-O-H(D) system in addition to the interactions attributed to oxygen and to the O-H(D) complex a third interaction is observed ν_{Q2}=220MHz which is present at all temperatures, is isotope independent and is stable in the temperature range studied. This interaction is not due to precipitation in ordered phases of the Nb-H system as it was not observed in a systematic phase diagram study of this system by perturbed angular correlations [Mendes 83, Gil 84,87a and 87b]. In order to clarify the origin of this interaction the sample loaded with deuterium was submitted to an isochronal annealing programme at 400K with an angular correlation measurement made at room temperature after each annealing stage. In Fig.5.9 is shown the dependence on the annealing time of the fraction of ν_{Q2} which decreases linearly and vanishes after an annealing time of 40 minutes. As this fraction decreases the fraction of the oxygen interaction increases by the same amount indicating that ν_{Q2} is converted to the oxygen interaction by the annealing procedure. Low temperature measurements after this procedure showed that the O-D interaction is still present at 80K as before and with a similar fraction.

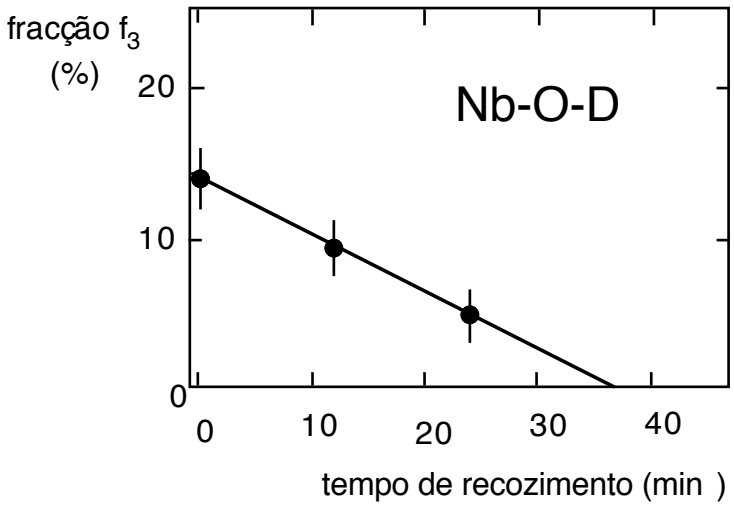

Fig. 5.9 - Fraction of probe atoms perturbed by the interaction ν_Q=220MHz, η=0.85 as a function of the annealing time at 400K for a deuterium loaded sample.

From the results of this experiment we may conclude that the complex responsible for ν_{Q2} is very stable and dissociates irreversibly after annealing at 400K and that this complex must be due to more than one hydrogen or deuterium atom trapped by oxygen.

The assignment of this interaction to trapping of more than one hydrogen atom by oxygen seems to contradict the well established fact that only one hydrogen atom is trapped by either oxygen or nitrogen in niobium [Pfeiffer 76, Sado 82]. This contradiction may be explained if we consider that oxygen is not isolated in the metal but trapped in the vicinity of the hafnium probe. This changes the potential which influences hydrogen and may lead, under favourable conditions, to the trapping of more than one hydrogen atom. However under normal conditions, for the concentrations, studied the formation of these complexes is highly unlikely and will require high local concentrations of hydrogen in the vicinity of the Hf-O complex. As refered before in the hydrogen loading process by electrolysis the elec-

tric contact between the sample and the external electric circuit is made by a gold wire in contact with the sample in several points. It is possible that when diffusing along the preferred paths determined by this configuration high local hydrogen concentrations exist in the sample giving rise to the necessary conditions for the formation of these complexes. The number of atoms affected by these complexes must therefore remain constant with temperature, as is experimentally observed, and the dissociation process will be irreversible since the conditions for their formation are no longer repeated. On the other hand as the mobility of deuterium is smaller than that of hydrogen a greater number of probe atoms should be affected in the case of deuterium, this is also observed experimentally. This process is not seen in Ta-O samples which indicates that hafnium may play an important role in the formation of these complexes favouring it in niobium.

The two interactions due to the presence of hydrogen in the Ta-N-H system show similar behaviours, their fractions are similar and they vanish at the same temperature. The interaction frequencies are similar (240MHz and 250MHz) however the large difference of the asymmetry parameters (0.80 and 0.40) shows that the configurations of the complexes causing these interactions must be different. As both interactions are only present after loading with hydrogen and as they are the same for deuterium they are caused by trapping of these atoms at nitrogen. Considering that in the Ta-O-H system trapping of hydrogen increases the value of η (Fig.5.10) and as we expect the configuration of the N-H complex to be similar to the O-H complex [Wipf 82] the interaction with η=0.80 must be due to trapping of one hydrogen in the same position as for oxygen. The other interaction may correspond to trapping of one hydrogen with a different configuration or to trapping of more than one hydrogen atom.

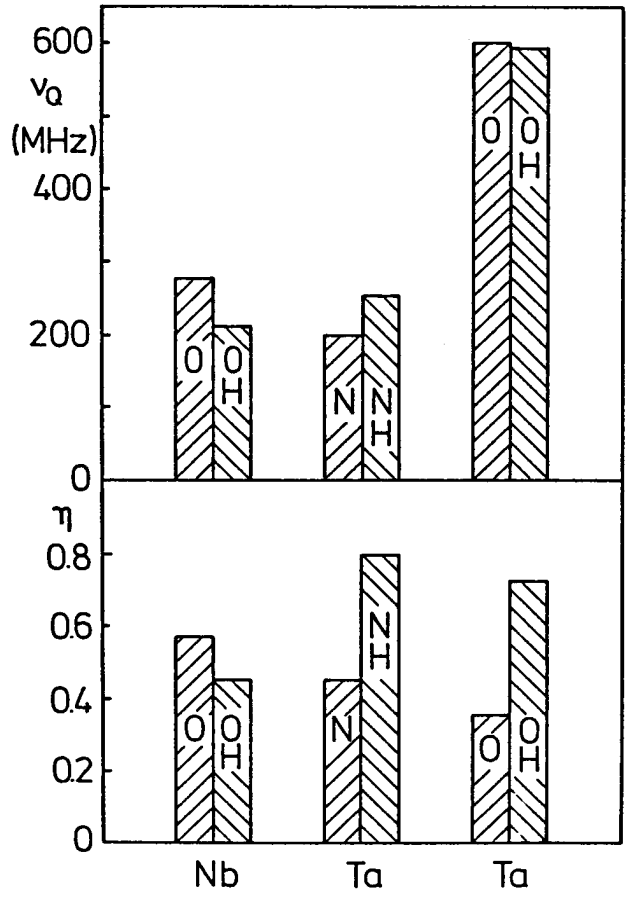

Fig. 5.10 - Bar chart with the interaction parameters for oxygen, nitrogen and their complexes with hydrogen in niobium and tantalum.

As the trapping of more than one hydrogen is unlikely and as the two interactions disappear simultaneously the hypothesis that a single hydrogen is trapped at another position is the most probable.

5.3.2 - The asymmetry parameters η

In order to find trends in the values of the asymmetry parameters these were calculated with the help of the point charge model described in section

2.5. The values for the positions and charges of oxygen in niobium and tantalum of the previous chapter were used and hydrogen atoms were placed in the positions suggested by other researchers [Magerl 83] as is shown in Fig.5.11. The charge placed in the hydrogen atom was adjusted in order to reproduce the experimental value of η in the O-H system in niobium (q=+0.72e). Calculations for tantalum were then performed only with a symmetrization of the oxygen-lattice atoms bonds and leaving the rest identical. The value of η for the complex O-H obtained, η=0.82, is high relative to the experimental value of 0.72 but the trend is correct. For any other positions of the oxygen and hydrogen atoms relative to hafnium in order that hydrogen is 4^{th} nearest neighbour to oxygen the value obtained for η is always of the order of 0.35, therefore only the position indicated in Fig.5.11 may justify the large increase of this parameter. According to Tab.5.1 we may see that, both for niobium and tantalum, the trend of the interaction frequencies when oxygen traps hydrogen is the same as observed experimentally. The point charge model fails however when the values for tantalum and niobium are compared.

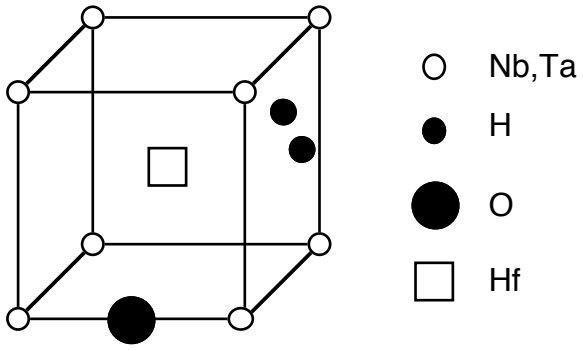

Fig. 5.11- Bcc unit cell showing the relative positions of the probe atom, oxygen and the two tetrahedral positions occupied by hydrogen.

Tab. 5.1- Theoretical values for ν_Q and η obtained with the point charge model for oxygen and for O-H complexes in niobium and tantalum. The first value for each complex corresponds to ν_Q and the second to η. The ratios between the experimental interaction frequencies and the theoretical values are shown in the last columns. The hydrogen charge is placed as indicated in Fig.5.11 and was adjusted in order to reproduce the experimental value of η for the system Nb-O-H. The values of ν_Q are in MHz.

	O	O-H	$\frac{\nu_{Q_O}}{\nu_{Q_{OH}}}$	$\frac{\nu_{Q_O}}{\nu_{Q_{OH}}}$(exp.)
Ta	-1571 0.31	-1387 0.82	1.13	1.23
Nb	-2447 0.57	-2120 0.48	1.14	1.32

We should expect a similar behaviour for nitrogen, that is, the value of η for the N-H complex in tantalum should be larger than for nitrogen alone and that is what is experimentally observed. The reverse should happen in niobium, the value of η for N-H should be smaller than that for nitrogen. The parameters of the N-H interaction were not determined in this work due to difficulties in obtaining samples with only the nitrogen interaction present.

5.3.3 - Temperature dependence of the defect fractions

The temperature dependence of the fractions of trapped hydrogen atoms may be interpreted in terms of trapping models. In the following sections we shall consider three distinct models.

5.3.3.a -Classical thermodynamical equilibrium

From a classical point of vue hydrogen in dilute solution in metals may be described considering that it behaves as a gas. In the presence of trapping defects the number of trapped hydrogen atoms, when thermodynamical equilibrium is reached, will be a function of the defect and hydrogen concentrations, the number of trapping sites per defect, the maximum number of hydrogen atoms that each defect may trap and of the competition between different types of defects.

Pfeiffer and Wipf developed such a model to determine the binding energy of hydrogen to nitrogen in niobium [Pfeiffer 76]. In this model two distinct situations are considered leading to different behaviours: in the first case the hydrogen concentration is smaller or equal to the nitrogen concentration and in the second case it is larger.

When the hydrogen concentration is smaller than that of nitrogen and the temperature is lowered all hydrogen atoms are trapped and no precipitates are formed. Considering that the interstitial impurity concentrations are very small there is no superposition of trapping sites belonging to different nitrogen atoms and the interaction between free hydrogens is small, and also that only a limited number of hydrogen atoms may be trapped by each nitrogen, the concentration c_t of trapped hydrogen atoms is given by [Pffeifer 76]:

$$c_t = \frac{1}{2}\left\{ c_H + q\,c_N + \frac{\lambda\, q}{z}\, e^{-\frac{\varepsilon}{kT}} - \left[\left(c_H + q\,c_N + \frac{\lambda\, q}{z}\, e^{-\frac{\varepsilon}{kT}} \right)^2 - 4\,q\,c_H\,c_N\right]^{\frac{1}{2}} \right\} \qquad (5.1)$$

where c_H and c_N are the hydrogen and nitrogen concentrations in the sample, q is the number of hydrogen atoms which may be trapped by each nitrogen, λ is the number of trapping sites per lattice atom, z is the number of trapping sites for each nitrogen atom, ε is the binding energy of hydrogen to nitrogen, k is the Boltzmann constant and T the absolute temperature.

In the present work only the samples used in the study of the Nb-O-H and Ta-N-H systems had a hydrogen concentration smaller than the interstitial impurity. In both systems the temperature at which the number of trapped hydrogen is 50% of their low temperature concentration is 80K. If we use this value for T in (5.1) and with λ=6, z=12 and q=1, the binding energy for this concentration ratio is ε=0.028eV, much smaller than the binding energies determined by other methods for these systems; ε=0.08eV for O-H in niobium [Hanada 81b] and ε=0.12eV for N-H in tantalum [Rosan 76]. The parameter λ corresponds to the number of interstitial tetrahedral sites per atom in the bcc lattice. The parameter z is determined from geometrical considerations based in the proposed trapping sites suggested by Wipf [Wipf 82]; anyway the ε dependence on z is weak and does not justify the difference between the experimental values of the binding energy and the values calculated with this model. The value of q must be equal to unity in all systems studied. According to (5.1) the temperature dependence of the hydrogen concentration

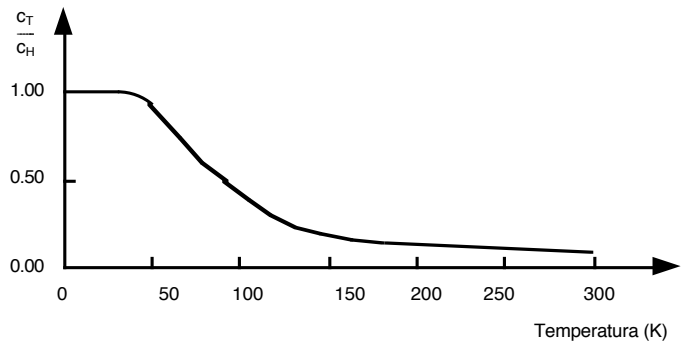

Fig. 5.12- Temperature dependence of the relative trapped hydrogen atoms in the Pfeiffer and Wipf model [Pfeiffer 76] in the absence of precipitates.

decreases slowly and even reaches an almost stable value at higher temperatures (see Fig.5.12). This behaviour is not in agreement with the present results as can be seen in Figs. 5.3 and 5.6.

When the hydrogen concentration is larger than that of oxygen (or nitrogen), as in the Ta-O-H(D) and Nb-O-H(D) systems, this model considers that each oxygen atom will trap one hydrogen and the excess hydrogen will precipitate in ordered phases. In this case the trapped hydrogen concentration is given by [Pfeiffer 76]:

$$c_t = \frac{c_0\, q\, c_N}{c_0 + \frac{\lambda\, q}{z}\, e^{\frac{(\Delta H-\varepsilon)}{k\,T}}} \qquad (5.2)$$

where ΔH is the precipitate binding energy and c_0 is a constant with the value c_0=4.7±0.9 for hydrogen in niobium. For N-H in niobium the binding energy to nitrogen is higher than the binding energy to precipitates [Sado 82] and the same should happen for the other complexes studied since we always see trapped

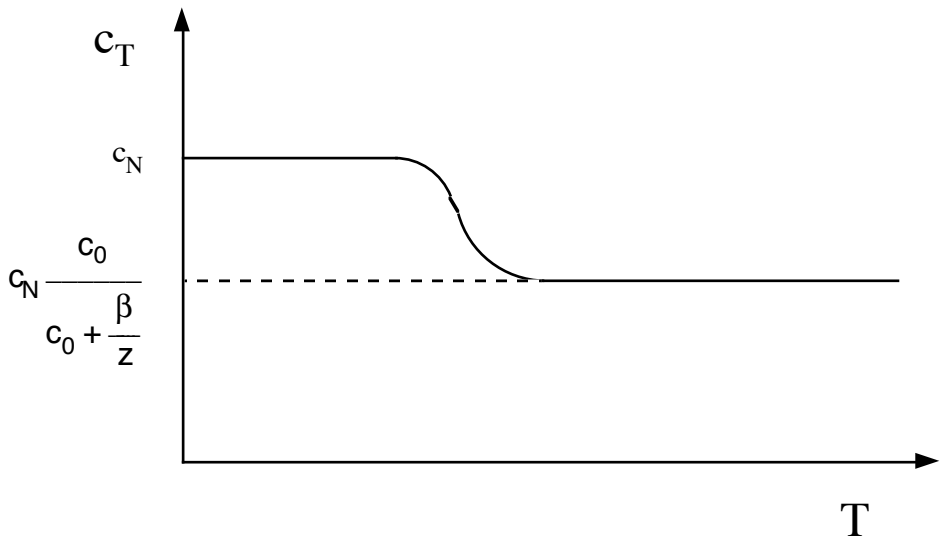

Fig. 5.13- Typical temperature dependence of the relative fraction of trapped hydrogen atoms in the presence of precipitates according to the model of Pfeiffer and Wipf [Pfeiffer 76].

hydrogen and no precipitates are observed. The behaviour of the hydrogen concentration predicted by the model according to (5.2) is represented in Fig.5.13. According to this model the concentration of hydrogen at high temperatures shows a relatively high constant value. For hydrogen in niobium and with λ=5 and z=1 the minimum value reached by c_t is of the order of 45% of the maximum which again is in disagreement with the present results. Therefore this model is not suitable for the interpretation of our results.

Cannelli [Cannelli 85] has described a more generalysed model which may be applied to definite geometries; however the occurrence of precipitates was not considered and the concentration of trapped hydrogen varies very slowly with temperature, therefore this model is also not suitable for the present results.

As the observed behaviour of trapped hydrogen is much different from the one found by other methods, particularly the lower temperature at which hydrogen is released and therefore the lower binding energies, we

conclude that hydrogen can not be considered to be bound only to oxygen or nitrogen. The presence in the vicinity of the complex of the radioactive probe (^{181}Hf) which is also an impurity in both metals may affect the behaviour of trapped hydrogen. Contrary to what was suggested in chapter 4 now the existence of hafnium before the angular correlation is no longer forgotten when the angular correlation is measured since now the lifetime of the first state of the cascade is of the same order of magnitude as the mean time of stay of hydrogen (or deuterium) in an interstitial position. On the other hand if hydrogen moves away from the ^{181}Ta-O(N) complex before the angular correlation is measured then this will only be affected by oxygen or nitrogen. However after

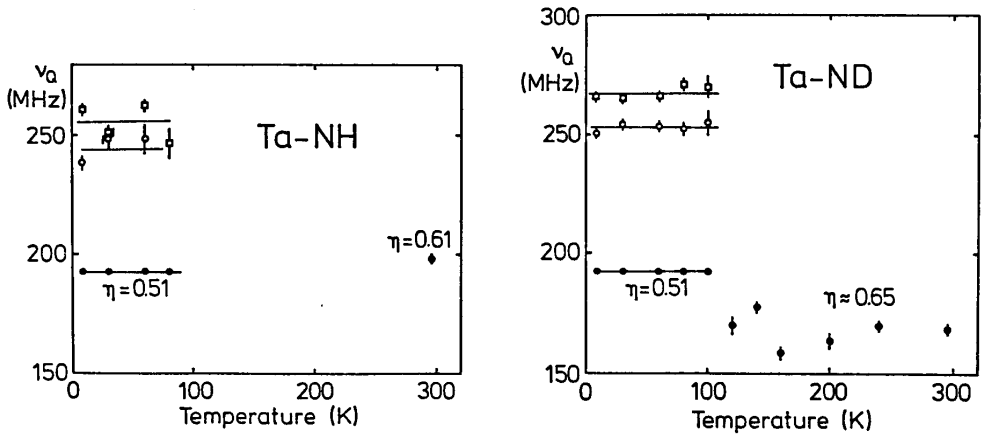

Fig.5.14 - Temperature dependence of the interaction frequencies observed in tantalum with nitrogen and hydrogen or deuterium. After the low temperature interaction disappears the interaction parameters of the nitrogen interaction deviate from their known values of ν_Q=192MHz and η=0.50.

the O-H (or N-H) interaction has vanished we observe that the oxygen or nitrogen interaction is different from it's well known value even at high temperatures as is shown, for instance, for the Ta-N-H(D) system in Fig.5.14. This suggests that hydrogen is bound to the Hf-O complex before it's decay and that the disappearance of the low temperature interaction is related to a rearrangement of hydrogen in the vicinity of oxygen but in a more distant position from the radioactive atom ^{181}Ta. It may be shown with the point charge model that if hydrogen is released when hafnium decays, but remains in the vicinity of oxygen occupying a position opposed to that of hafnium, the electric field gradient due to this charge distribution is approximately the same as that created by oxygen alone. The two models presented in the next sections are based in these considerations.

5.3.3.b - Thermodynamical equilibrium with trapped hydrogen

After the previous considerations it is reasonable to suppose that the crystal potential affecting hydrogen in the vicinity of the probe atom-interstitial impurity has several trapping wells around oxygen and a deeper one close to hafnium (Fig.5.15). In thermodynamical equilibrium, supposing that for each "trapped" state bound to the Hf-O complex (i in fig.5.15) there are s "free" states bound only to oxygen, then the probability of finding one free hydrogen is proportional to the product of a Boltzmann factor by the number of states available, while the probability of hydrogen being trapped is constant:

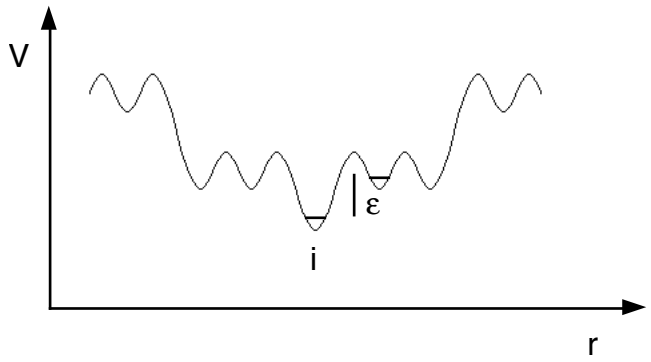

Fig. 5.15 - Suggested crystal potential affecting the hydrogen atom for the trapping models.

$$P(\text{livre}) \quad \alpha \; r \; e^{-\frac{\varepsilon}{kT}}$$
$$P(\text{capturado}) \quad \alpha \; 1 \qquad (5.3)$$

where ε is the energy difference between the trapped and the free state.

At very low temperatures all hydrogen atoms are trapped. When the temperature is raised the fraction of trapped atoms is given by:

$$\frac{f}{f_0} = \frac{1}{1 + s\, e^{-\frac{\varepsilon}{kT}}} \qquad (5.4)$$

where f_0 is the fraction of trapped hydrogen atoms when the temperature goes to zero. From (5.4) it follows:

$$\ln\left(\frac{f_0}{f} - 1\right) = \ln s - \frac{\varepsilon}{kT} \qquad (5.5)$$

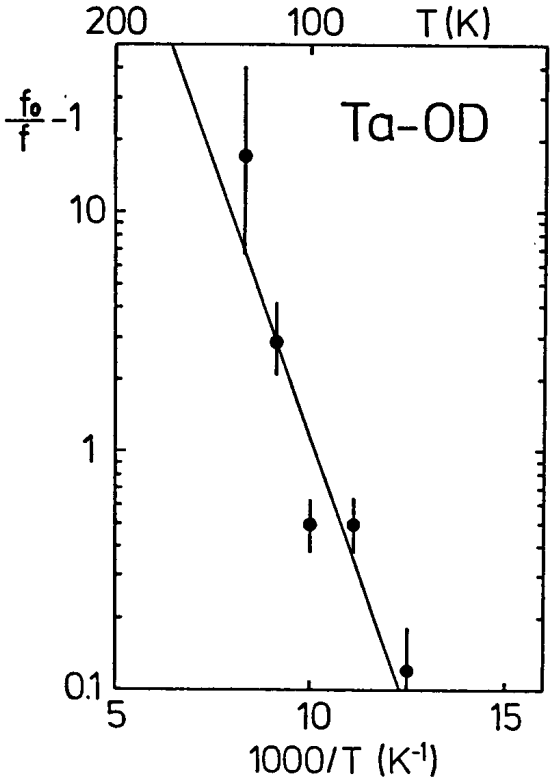

Fig. 5.16- Relative fraction of O-D complexes in tantalum as a function of the inverse temperature according to the trapping model of section 5.3.3.b. The straight line is a fit of (5.5) to the experimental data.

In Fig.5.16 the values of (f_0/f-1) as a function of 1/T are plotted for the Ta-O-D system. The straight line is a fit of (5.5) to the experimental data with:

$$\varepsilon = 94 \text{ meV} \qquad \text{and} \qquad s = 7 \times 10^4 \tag{5.6}$$

and similar values for the other systems. Although the binding energy is of the same order of magnitude as the experimental values already known the value of s is too high. Since s is the ratio of free and trapped states around the Hf-O complex, values of the order of 10 would be expected. Therefore this model is not adequate for our results.

5.3.3.c - Hydrogen released by the nuclear decay

In the previous model the decay of hafnium does not alter the crystal potential of Fig.5.15 affecting hydrogen. In this model we shall suppose that trapping of hydrogen close to hafnium only exists before the decay and that hafnium releases hydrogen of the trapped state after decay. This is equivalent to the disappearance of the potential well i in Fig.5.15 after the decay. If we assume that the probability of hydrogen remaining in the same position after the decay varies exponentially with time:

$$P(t=0) = 1$$

$$P(t=t) = e^{-\frac{t}{\tau}} \qquad (5.7)$$

e

Where τ is the mean time of stay of hydrogen in a trapped position at the temperature T, Then the probability that, when the angular correlation is observed at time t, hydrogen is still trapped is given by:

$$P_0(t) = e^{-\frac{t}{\tau}} \frac{e^{-\frac{t}{\tau_N}}}{\tau_N} \qquad (5.8)$$

where $(1/t_N \; e^{-t/\tau_N})$ is the probability of detecting the second γ-ray at the time t after hafnium decays with τ_N the lifetime of the ^{181}Ta excited state populated by the hafnium decay.

In the region of temperatures where the hydrogen or deuterium interaction vanishes, the ratio between this fraction and it's value for very low temperatures f/f_0 is given by the integral of $P_0(t)$ from 0 to ∞:

$$\frac{f}{f_0} = \frac{1}{\tau_N} \int_0^{\infty} e^{-\frac{t}{\bar{\tau}}} e^{-\frac{t}{\tau_N}} dt \qquad (5.9)$$

calculating the integral in (5.9) we get:

$$\frac{f}{f_0} = \frac{\bar{\tau}}{\bar{\tau} + \tau_N} \qquad (5.10)$$

from where follows:

$$\bar{\tau} = \frac{\tau_N}{\frac{f_0}{f} - 1} \qquad (5.11)$$

If we assume that τ has an Arrhenius behaviour in this temperature range:

$$\bar{\tau} = \tau_\infty e^{\frac{\varepsilon}{\kappa T}} \qquad (5.12)$$

we find:

$$\frac{1}{\frac{f_0}{f} - 1} = \frac{\tau_\infty}{\tau_N} e^{\frac{\varepsilon}{kT}} \qquad (5.13)$$

From where we find:

$$\ln\left(\frac{f_0}{f} - 1\right) = \ln\frac{\tau_N}{\tau_\infty} - \frac{\varepsilon}{kT} \qquad (5.14)$$

From (5.14) values for the binding energy ε and for the time of stay τ_∞ of hydrogen (deuterium) when the temperature goes to infinity can be obtained. In Tab.5.2 values for ε and τ_∞ calculated with (5.14) for the systems studied are presented. In Figs.5.17 and 5.18 the dependence of τ as a function of 1/T obtained experimentally are plotted against the known values for hydrogen and deuterium in tantalum and niobium [Qi 83]. The dashed lines are an extrapolation from the high temperature region.

The values of ε and τ_∞ obtained with oxygen and nitrogen in tantalum are similar for the two isotopes which indicate that both atoms create similar potentials. The values of ε and τ_∞ in niobium are identical as is expected from the similar behaviour of these two systems. The activation energies obtained with this model correspond to approximately 30-50% of the binding energies to oxygen or nitrogen in pure systems.

Tab. 5.2- Energy activation ε and time of stay τ_∞ when T goes to ∞ for the nuclear model of section 5.3.3.c.

		ε (mev)	τ_∞ (10^{-9}s)
Nb	H(D)	39 ± 23	155 ± 16
Ta	H	28 ± 4	62 ± 2
	D	57 ± 18	32 ± 1

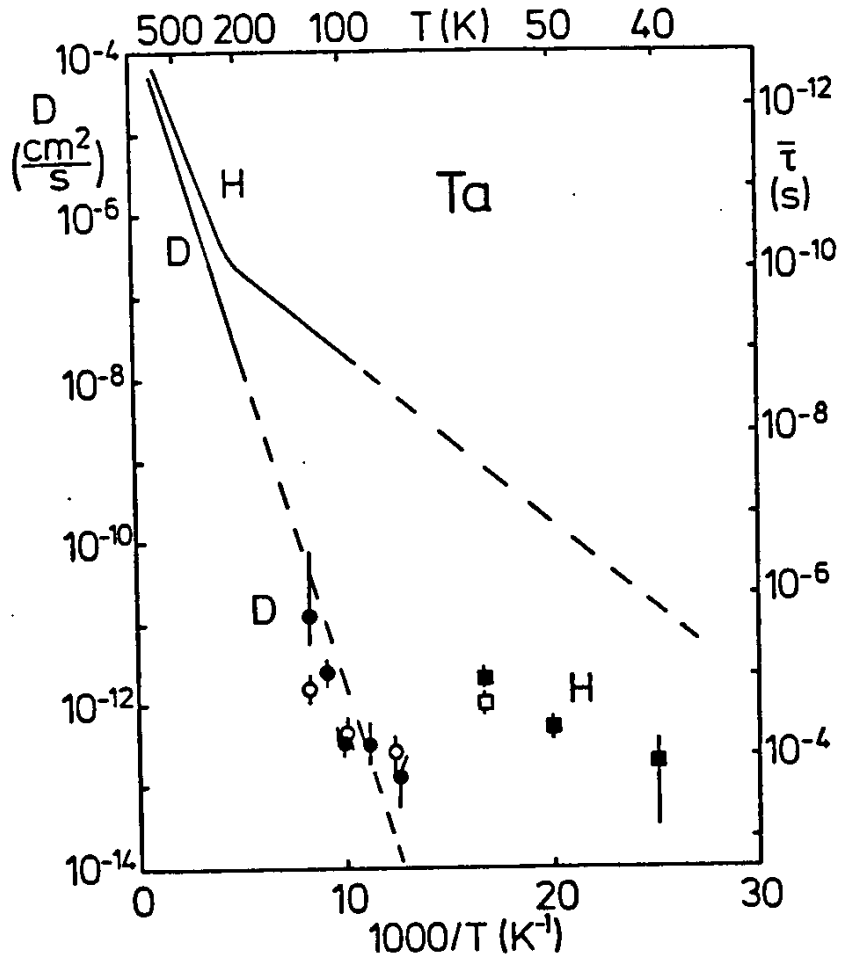

Fig. 5.17- Values for the mean time of stay of hydrogen and deuterium trapped by oxygen (black symbols) and by nitrogen (white symbols) in tantalum according to the nuclear model of section 5.3.3.c compared with the diffusion data available. The dashed lines are extrapolations of the high temperature data.

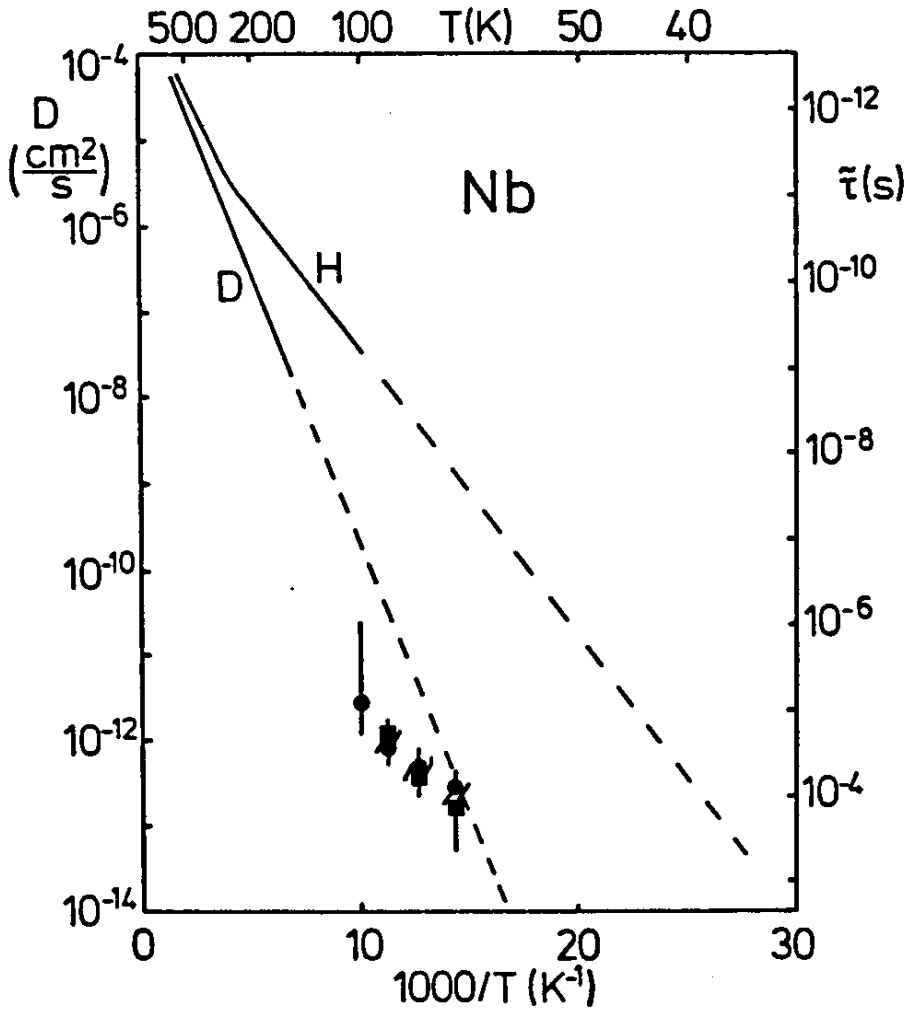

Fig. 5.18- Values for the mean time of stay of hydrogen and deuterium trapped by oxygen (black symbols) and by nitrogen (white symbols) in niobium according to the nuclear model of section 5.3.3.c, compared with the diffusion data available. The dashed lines are extrapolations of the high temperature data.

From Figs.5.17 and 5.18 we may see that the diffusibility of hydrogen (deuterium) when trapped is smaller than the extrapolated values of diffusion for free atoms particularly in the case of hydrogen. On the other hand the diffusivity values obtained with this model are not much different from extrapolations of the values observed by Qi et all [Qi 83] for hydrogen and deuterium diffusion in the presence of interstitial nitrogen.

5.4 - Conclusions

From the studies of hydrogen and deuterium complexes with oxygen and nitrogen in niobium and tantalum we may conclude that:

- Under normal circunstances only one hydrogen or deuterium atom is trapped by the interstitial impurities oxygen and nitrogen confirming the results of other experiments with macroscopical techniques.
- In niobium the temperature at which these interactions vanish is the same for both isotopes. This behaviour is attributed to the fact that, as opposite to tantalum, both the probe atom and the product of it's decay are impurities in this metal.
- In some systems other interactions are observed also due to hydrogen and with similar behaviour for the two isotopes. In the Nb-O system an interaction is observed which is due to meta-stable hydrogen complexes formed during the electrolytical loading and which disappear after annealing at 400K. In the Ta-N system one interaction probably due to a different configuration of the N-H(D) complex is also observed.
- The relative values of the η parameter for the O-H(D) complex interaction in tantalum may be understood in terms of a simple point charge model if we consider the covalent bonding charges of oxygen delocalized and oriented according to the crystal symmetry. This model agrees with the positions suggested for hydrogen by other researchers [Wipf 82, Magerl 83] with hydrogen occupying tetrahedral sites 4^{th} nearest neighbours to oxygen or nitrogen.
- It was not possible to identify the interaction due to the N-H complex in niobium since we were unable to isolate the nitrogen interaction. Suppression of the interactions due to complexes of more than one nitrogen

requires changing the loading procedure in order to achieve higher cooling rates to freeze the random distribution of nitrogen atoms in the α phase and preventing precipitates.

- Trapping models were used for the interpretation of the temperature dependence of the fractions of hydrogen atoms trapped. The classical point of vue of thermodynamical equilibrium between trapped and free states is unable to describe the present results as the binding energies calculated are very low when compared to results of other techniques and also because the temperature dependence of the fractions of trapped atoms is in disagreement with experiment. The results were therefore interpreted in terms of hydrogen diffusing away from the radioactive probe but remaining in the vicinity of the interstitial impurity. In particular we find values of the mean time of residence for these atoms which are between extrapolations of high temperature data of the metal-hydrogen pure systems and the metal-hydrogen(deuterium)—oxygen(nitrogen) systems.

CHAPTER 6

FINAL REMARKS

The results of the present work show that the perturbed angular correlation method may be used for the study of hydrogen in metals with some advantages over the more common macroscopic methods. The identification of each type of defect by a unique interaction allows the study of it's evolution even when other interactions are present. This feature was used successfully in the present work in the studies of the Nb-O-H(D) systems.

However when the number of interactions, or types of defects, is high as in the Nb-N-H(D) systems the fitting procedures of the theoretical perturbation function to the experimental data becomes difficult not allowing a unique attribution of the interactions present. The possibility of hydrogen being captured by each of the three types of defects observed in the Nb-N system, with the possibility of the existence of different configurations for the same defect, leads to a large number of interactions which difficults the unambiguous and coherent fit of the different experimental spectra.

The identification and study of the interaction due to the N-H complex in niobium is interesting since this is one of the most extensively studied systems. For this purpose a better control of the nitrogen dilution in niobium is necessary in particular the cooling rate must be fast enough to

quench the random solution of nitrogen atoms in the metal without the occurrence of precipitates.

Although the present results agree with the position of hydrogen relative to oxygen or nitrogen as suggested by Magerl et all [Magerl 83] for niobium (according to the calculations of the point charge model), it would be interesting to investigate the symmetry of these defects by studying them in single crystals. The Ta-O-H system is the most convenient for these studies as it is easy to prepare and the only interactions observed are due to oxygen and to the O-H complex. Furthermore the probe atom after the decay is similar to the lattice atoms. However this experiment involves the implantation of the radioactive species in a tantalum single crystal.

Within the scope of this project studies of inelastic X-Ray scattering in the Ta-O-H system are planned. This method has recently been used to study the symmetry and lattice distortions caused by N-H complexes in niobium [Metzger 85].

As a natural development of the hydrogen in metals project in which this work is included studies of perturbed angular correlations in hydrogenated alloys of technological importance such as $LaNi_5$ and FeTi is being planned.

APPENDIX A

THE PERTURBED ANGULAR CORRELATION AND THE ELECTRIC HYPERFINE INTERACTION

A.1 - The Perturbed Angular Correlation

The general form of the angular correlation between two γ rays emitted successively by an excited nucleus in the absence of extra nuclear perturbations (fig.2.1) is given by [Frauenfelder 65]:

$$W(\mathbf{k}_1,\mathbf{k}_2) = \sum_{\substack{m_i\ m_a\ m_b \\ m'_a\ m'_b\ m_f}}{}' <m_f|H_2|m_b><m_a|H_1|m_i>\delta_{m_a m_b} \times <m_f|H_2|m'_a>^{*}<m'_b|H_1|m_i>^{*}\delta_{m'_a m'_b} \qquad (A.1)$$

where the Hamiltonians H_1 and H_2 describe the interaction of the nucleus with the radiation field. Without extra nuclear perturbations during the lifetime of the intermediate state the final eigenstates $|m_a>$, $|m'_a>$ after the emission of γ_1 are identical to the initial eigenstates $|m_b>$, $|m'_b>$ of the second radiation γ_2.

We now consider that the nucleus is no longer isolated but interacts with an extra nuclear electromagnetic field. This interaction, characterized by an Hamiltonian K, will affect the nucleus during the time interval be-

tween the emission of γ_1 (t=0) and the emission of γ_2 (t=t). During this time interval the external field interacts with the nuclear moments of the intermediate state giving rise to transitions from the magnetic substates $|m_a\rangle$ to different substates $|m_b\rangle$. The time evolution of these states is represented by a unitary operator $\Lambda(t)$ satisfying Schrödinger equation:

$$\frac{\partial}{\partial t}\ \Delta\ (t)\ =\ -\ \frac{i}{h} K\ \Delta\ (t) \qquad (A.2)$$

For time independent interactions, K does not depend on time and the solution to (A.2) is simply:

$$\Delta\ (t)\ =\ e^{-\frac{i}{h} K\, t} \qquad (A.3)$$

Therefore the perturbed angular correlation is given by:

$$W(\mathbf{k}_1,\mathbf{k}_2)\ =\ \sum_{\substack{m_i\ m_f\\ m_a\ m'_a}} \langle m_f|H_2\Delta(t)|m_a\rangle\langle m_a|H_1|m_i\rangle\ \times\ \times\ \langle m_f|H_2\Delta(t)|m'_a\rangle^{*}\ \langle m'_a\ |H_1|m_i\rangle^{*} \qquad (A.4)$$

The states $|m\rangle$ form a complete set and the state vector $\Lambda(t)\ |m_a\rangle$ may be expanded in terms of this base:

$$\Delta\ (t)\ \ |m_a\rangle\ =\ \sum_{m_b}\ |m_b\rangle\langle m_b|\ \Delta(t)\ |m_a\rangle$$

$$\Delta\ (t)\ \ |m'_a\rangle\ =\ \sum_{m'_b}\ |m'_b\rangle\langle m_b|\ \Delta(t)\ |m_a\rangle \qquad (A.5)$$

After this expansion the angular correlation may be written:

$$W(\mathbf{k}_1,\mathbf{k}_2,t) = \sum_{\substack{m_i\ m_f\\ m_a m'_a\\ m_b m'_b}} \langle m_f|H_2|m_b\rangle\langle m_b|\Delta(t)|m_a\rangle\langle m_a|H_1|m_i\rangle \times \qquad (A.6)$$
$$\times \langle m_f|H_2|m'_b\rangle^*\langle m'_b|\Delta(t)|m'_a\rangle^*\langle m'_a|H_1|m_i\rangle^*$$

A comparison of (A.1) with (A.6) shows that the perturbed angular correlation may be written as the product of the matrix elements of the unperturbed correlation by time dependent matrix elements describing the influence of the extra nuclear interaction on the angular correlation.

Finally the perturbed angular correlation (A.6) may be conveniently written:

$$W(\mathbf{k}_1,\mathbf{k}_2,t) = \sum_{\substack{k_1\ k_2\\ N_1\ N_2}} A_{k_1}(1)\,A_{k_2}(2)\,G^{N_1N_2}_{k_1k_2}(t)\,[(2k_1+1)\,(2k_2+1)]^{\frac{1}{2}}\,Y^{N_1*}_{k_1}(\theta_1,\varphi_1)\,Y^{N_2*}_{k_2}(\theta_2,\varphi_2) \qquad (A.7)$$

with the perturbation factor given by:

$$G^{N_1N_2}_{k_1k_2}(t) = \sum_{m_a\ m_b} (-1)^{2I+m_a+m_b}\,[(2k_1+1)(2k_2+1)]^{\frac{1}{2}} \begin{pmatrix} I & I & k_1\\ m'_a & -m_a & N_1\end{pmatrix}\begin{pmatrix} I & I & k_2\\ m'_b & -m_b & N_2\end{pmatrix} \times$$
$$\times \langle m_b|\Delta(t)|m_a\rangle\langle m'_b|\Delta(t)|m'_a\rangle^* \qquad (A.8)$$

where k_1 and k_2 are the multipolarities allowed for γ_1 and γ_2, (θ_1,φ_1) and (θ_2,φ_2) are the Euler angles for the directions k_1 and k_2 as indicated in fig.A.1. For vanishing perturbation (t=0) the evolution matrix $\Lambda(t)$ reduces to the unit matrix and the orthogonal relations of the 3-j symbols gives:

$$G_{k_1 k_2}^{N_1 N_2}(t) \equiv \delta_{k_1 k_2}\ \delta_{N_1 N_2} \qquad (A.9)$$

Therefore (A.7) for the unperturbed angular correlation reduces to:

$$W(\theta,t) = \sum_k A_k^{(1)}(L_1,L_1',I_i,I)\ A_k^{(2)}(L_2,L_2',I,I_f)\ \ P_k(\cos\theta) \qquad (A.10)$$

Where $A_k(1)$ describes the radiation γ_1 emitted between the initial state I_i and

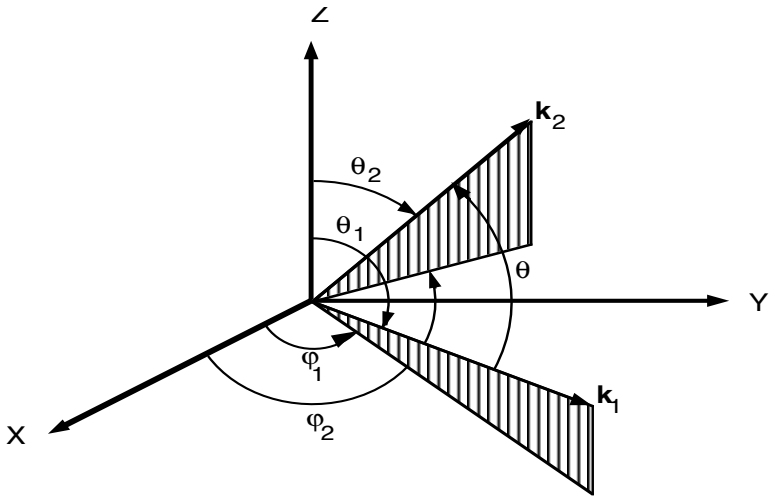

Fig. A.1- Euler angles for k_1 e k_2.

the intermediate state I, $A_k(2)$ describes the radiation γ_2 emitted between the intermediate state I and the final state I_f (see fig.2.1) and θ is the angle between the two directions k_1 and k_2.

For angular correlations observed in a cylindrical symmetry and in a polycrystalline sample (A.7) reduces to:

$$W(\theta,t) = \sum_{k=0}^{k_{max}} A_{kk}\ G_{kk}(t)\ P_k(\cos\theta) \qquad (A.11)$$

where $A_{kk}=A_k(1)A_k(2)$.

A.2 - The Electric Quadrupole Interaction

To determine the matrix elements of the perturbation in (A.8) a knowledge of the electrostatic Hamiltonian, H_{el}, responsible for the hyperfine interaction is essential.

A.2.1 - Classical Hyperfine Interaction

The electrostatic energy of the nuclear charge, described by $\rho_n(r)$ under the influence of the potential V(r), created by the electrons and the lattice charges, is given by:

$$W = \int \rho_n(\mathbf{r})\ V(\mathbf{r})\ d\tau \qquad \text{(A.12)}$$

with

$$Ze = \int r_n(\mathbf{r})\ dt \qquad \text{(A.13)}$$

the total nuclear charge.

Assuming that V(r) changes slowly in the region where $\rho_n(r)$ is non vanishing it may be expanded in a Taylor series in the vicinity of r=0:

$$V(\mathbf{r}) = V(0) + \sum_{\alpha=1}^{3}\left(\frac{\partial V}{\partial x_\alpha}\right)_0 + \frac{1}{2}\sum_{\substack{\alpha=1\\ \beta=1}}^{3}\left(\frac{\partial^2 v}{\partial x_\alpha \partial x_\beta}\right)_0 x_\alpha\, x_\beta + \ldots \qquad \text{(A.14)}$$

Inserting (A.13) and (A.14) in (A.12) the electrostatic energy is given by:

$$W = V_0 Z e + \sum_{\alpha=1}^{3} \left(\frac{\partial V}{\partial x_\alpha}\right)_0 \int \rho_n(\mathbf{r})\, x_\alpha \, d\tau + \frac{1}{2} \sum_{\substack{\alpha=1 \\ \beta=1}}^{3} \left(\frac{\partial^2 V}{\partial x_\alpha \partial x_\beta}\right)_0 \int \rho_n(\mathbf{r}) x_\alpha x_\beta \, d\tau + \ldots \quad (A.15)$$

The first term is the Coulomb energy of a point charge, which only contributes to the potential energy of the lattice and therefore has no relevance on the discussion of hyperfine interactions. The second term corresponds to the dipole interaction which vanishes for nuclear states with a well defined parity since the dipole moment for these states is zero. The third term includes the isomeric shift and the quadrupole interaction.

With $r^2=\sum x_\alpha^2$ the third term may be written as follows

$$W = \frac{1}{6} \int \rho_n(\mathbf{r}) r^2 d\tau \sum_{\substack{\alpha=1 \\ \beta=1}}^{3} \left(\frac{\partial^2 V}{\partial x_\alpha \partial x_\beta}\right)_0 + \frac{1}{6} \sum_{\substack{\alpha=1 \\ \beta=1}}^{3} \left(\frac{\partial^2 V}{\partial x_\alpha \partial x_\beta}\right)_0 \int \rho_n(\mathbf{r})(3x_\alpha x_\beta - r^2 \delta_{\alpha\beta})\, d\tau \quad (A.16)$$

The second derivatives $(\partial^2 V/\partial x_\alpha \partial x_\beta)=q_{\alpha\beta}$ form a symmetric (3x3) matrix which may be diagonalized by a convenient rotation of the coordinate system. Performing this rotation on the first term of (A.16) and considering that the electrostatic potential V(r) obeys the Poisson equation $\Delta V=-4\pi\rho_e(r)$, where $\rho_e(r)$ is the electronic charge density, in holding particularly for r=0 we get:

$$(\Delta V)_0 = \sum q_{\alpha\alpha} = 4\pi e |\psi(0)|^2 \quad (A.17)$$

where $e|\psi(0)|^2$ is the charge density of the electrons inside the nucleus.

The electrostatic hyperfine interaction is therefore:

$$W = \frac{2\pi e}{3} |\Psi(0)|^2 \int \rho_n(\mathbf{r})\, r^2\, d\tau + \frac{1}{6} \sum_{\substack{\alpha=1 \\ \beta=1}}^{3} \left(\frac{\partial^2 \phi}{\partial x_\alpha \partial x_\beta} \right)_0 \int \rho_n(\mathbf{r})\, (3x_\alpha x_\beta - r^2 \delta_{\alpha\beta})\, d\tau \qquad (A.18)$$

$$\equiv V(I) + V(Q)$$

The isomeric shift V(I) reflects the interaction between the extended charge of the nucleus and the electronic density at the nucleus.

The quadrupole term V(Q) gives the interaction between the electric field gradient tensor and the quadrupole moment tensor which describes the non spherical nuclear charge distribution.

A.2.2 - Quantum Mechanical treatment of the Electrostatic Hyperfine Interaction

The nuclear eigenstates may be characterized by the angular momentum quantum numbers I and m. In this representation the energy of the electrostatic interaction is given by the matrix element of the Hamiltonian:

$$E_m = \langle Im | H_{el} | Im \rangle \qquad (A.19)$$

with

$$H_{el} = \sum_{n,e} \frac{\rho_n \rho_e}{|r_n - r_e|} \qquad (A.20)$$

the sum is extended to all the nuclear, n, and extra nuclear, e, charges (fig.A.2).

Expanding (A.20) in Legendre polinomials

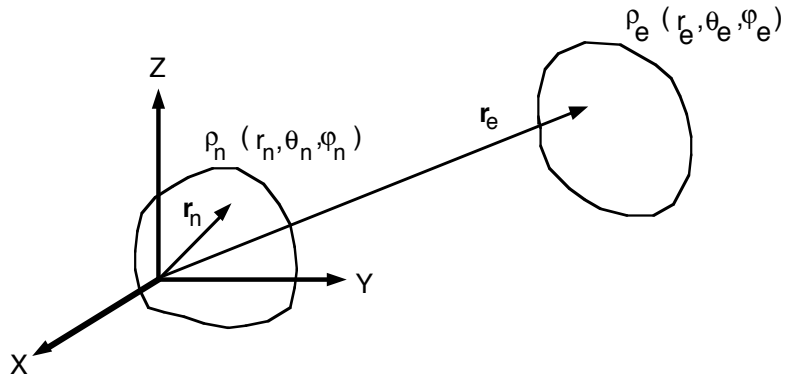

Fig. A.2- Nuclear, r_n , and extra nuclear, r_e , charge distributions.

$$\frac{1}{|\mathbf{r}_n - \mathbf{r}_e|} = \sum_{k=0}^{\infty} \frac{r_n^k}{r_e^{k+1}} P_k(\cos(\mathbf{r}_n,\mathbf{r}_e)) \quad ; \quad |r_e| > |r_n| \qquad (A.21)$$

and with the addition theorem for the spherical harmonics we find

$$H_{el} = 4\pi \sum_{k=0}^{\infty} \frac{1}{2k+1} \left[\sum_q (-1)^q \left(\sum_n \rho_n r_n^k Y_{k,q}(\theta_n,\varphi_n) \right) \left(\sum_e \frac{\rho_e}{r_e^{k+1}} Y_{k,q}(\theta_e,\varphi_e) \right) \right] \qquad (A.22)$$

This may be written in a more compact way by introducing the tensor operators for the nuclear moments $T_q^{(k)}$ and the external field $V_q^{(k)}$ (q is the rank of the tensor):

$$\begin{aligned} T_q^{(k)} &= \sum_n \rho_n \, r_n^k \, Y_{k,q}(\theta_n,\varphi_n) \\ V_q^{(k)} &= \sum_e \frac{\rho_e}{r_e^{k+1}} \, Y_{k,-q}(\theta_e,\varphi_e) \end{aligned} \qquad (A.23)$$

As the scalar product of two tensors of the same rank is given by

$$T^{(k)}\ V^{(k)} = \sum_{q=-k}^{+k} (-1)^q\ T_q^{(k)}\ V_q^{(k)} \qquad (A.24)$$

the Hamiltonian may be written

$$H_{el} = \sum_{k=0}^{\infty} \frac{4\pi}{2k+1}\ T^{(k)}\ V^{(k)} = 4\pi \left[\frac{Z\,e}{4\pi} V(0) + \frac{1}{3} \sum_{q=-1}^{+1} (-1)^q\, T_q^{(1)}\, V_q^{(1)} + \right.$$

$$\left. + \frac{1}{5} \sum_{q=-2}^{+2} (-1)^q\ T_q^{(2)}\ V_q^{(2)} + \frac{1}{7} \sum_{q=-3}^{+3} (-1)^q\ T_q^{(3)}\ V_q^{(3)} + \ldots \right] \qquad (A.25)$$

The first term is the Coulomb term. The expectation values of $T^{(1)}$ (electric dipole moment) and of $T^{(3)}$ (electric quadrupole moment) are zero. Higher order moments are usually very small and can be neglected. We are therefore left with the Hamiltonian operator for the electric quadrupole interaction:

$$H_{el} = \frac{4\pi}{5}\ T^{(2)}\ V^{(2)} = \frac{4\pi}{5} \sum_{q=-2}^{+2} (-1)^q\ T_q^{(2)}\ V_q^{(2)} \qquad (A.26)$$

The electric field gradient tensor $V^{(2)}$ can be expressed in an arbitrary cartesian coordinate system (x',y',z'). Taking into account it's symmetry

$$V_{\alpha'\beta'} = \frac{\partial^2 V}{\partial\alpha'\,\partial\beta'} = V_{\beta'\alpha'} \qquad (A.27)$$

and Laplace's equation $\Delta V = 0$ (considering only the charge distribution which is external to the nucleus) only five independent components remain expressed as:

$$V_0^{(2)} = \frac{1}{4}\sqrt{\frac{5}{\pi}}\, V_{z'z'}$$

$$V_{\pm 1}^{(2)} = \mp \frac{1}{2}\sqrt{\frac{5}{6\pi}}\, (V_{x'z'} \mp i\, V_{y'z'}) \qquad \text{(A.28)}$$

$$V_{\pm 2}^{(2)} = \frac{1}{4}\sqrt{\frac{5}{6\pi}}\, (V_{x'x'} - V_{y'y'} \pm 2V_{x'y'})$$

The number of components may be further reduced by a suitable transformation to the principal axis

$$V_0^{(2)} = \frac{1}{4}\sqrt{\frac{5}{\pi}}\, V_{zz}$$

$$V_{\pm 1}^{(2)} = 0 \qquad \text{(A.29)}$$

$$V_{\pm 2}^{(2)} = \frac{1}{4}\sqrt{\frac{5}{6\pi}}\, (V_{xx} - V_{yy})$$

If we define $\eta=(V_{xx}-V_{yy})/V_{zz}$ the electric field gradient is characterized as well by the parameters V_{zz} and η. With the convention $|V_{xx}|\leq|V_{yy}|\leq|V_{zz}|$ the asymmetry parameter η has values in the range $0\leq\eta\leq1$.

When the field gradient has axial symmetry, as for hexagonal or tetragonal lattices, the components V_{xx} and V_{yy} are equal and the electric field gradient is given by

$$V_0^{(2)} = \frac{1}{4}\sqrt{\frac{5}{\pi}}\, V_{zz} \qquad \text{(A.30)}$$

And the Hamiltonian reduces to:

$$H_{el} = \sqrt{\frac{\pi}{5}}\ T_0^{(2)}\ V_{zz} \qquad (A.31)$$

with the quadrupole interaction energy given by:

$$E_m = \langle Im| H_Q |Im\rangle = \sqrt{\frac{\pi}{5}}\ V_{zz} \langle Im| T_0^{(2)} |Im\rangle \qquad (A.32)$$

The quadrupole moment of the nucleus is defined as the maximum Z component (I=m) of the quadrupolar tensor

$$e\,Q = \langle II| \sum_n \rho_n (3z_n^2 - r_n^2) |II\rangle = 4 \sqrt{\frac{\pi}{5}}\ V_{zz} \langle Im| T_0^{(2)} |Im\rangle \qquad (A.33)$$

Using the Wigner-Eckart theorem (A.32) and (A.33) become:

$$E_m = (-1)^{I-m} \sqrt{\frac{\pi}{5}}\ V_{zz} \begin{pmatrix} I & 2 & I \\ -m & 0 & m \end{pmatrix} \langle I \| T^{(2)} \| I\rangle \qquad (A.32a)$$

$$e\,Q = 4 \sqrt{\frac{\pi}{5}}\ \begin{pmatrix} I & 2 & I \\ -I & 0 & I \end{pmatrix} \langle I \| T^{(2)} \| I\rangle \qquad (A.33a)$$

Where $\langle I \| T^{(2)} \| I \rangle$ is the reduced matrix element of the quadrupole moment operator.

By replacing (A.33a) in (A.32a) and evaluating the 3-j symbols we find for the quadrupole interaction energies of the m states:

$$E_m = \frac{3m^2 - I(I+1)}{4I\,(2I-1)}\ e\,Q\,V_{zz} \qquad (A.34)$$

From the properties of the 3-j symbols it follows that $E_m=0$ for $I<1$ and $E_m\neq0$ for $I>1$. As the energies depend on m^2 there remains a twofold degeneracy of the m states and the splitting between these substates is not equidistant.

The difference in energy between two substates m and m' is given by:

$$E_m - E_{m'} = \frac{3\, e\, Q\, V_{zz}}{4I\,(2I-1)} \left| m^2 - m'^2 \right| \qquad (A.35)$$

If we define the quadrupole frequency as:

$$\omega_Q = \frac{e\, Q\, V_{zz}}{4I\,(2I-1)\,h} \qquad (A.36)$$

we get:

$$E_m - E_{m'} = 3\, h\, \omega_Q \left| m^2 - m'^2 \right| \qquad (A.37)$$

The transition frequency ω_0 corresponding to the smallest measurable energy difference is:

$$\begin{aligned} \omega_0 &= 3\, \omega_Q \qquad \text{for I integer} \\ \omega_0 &= 6\, \omega_Q \qquad \text{for I half-integer} \end{aligned} \qquad (A.38)$$

A.2.3 - The Perturbation Factor for the Electric Quadrupole Interaction

The matrix elements $\langle m_i|L(t)|m_j\rangle$ of the perturbation factor (A.8) can be calculated if we replace K in (A.3) by the Hamiltonian H_{el} (A.31):

$$\langle m_b|\Delta(t)|m_a\rangle = \langle m_b|e^{-\frac{i}{h}H_{el}t}|m_a\rangle = e^{-\frac{i}{h}E_{m_b}t}\delta_{m_a m_b} \qquad (A.39)$$

and similarly for m'_a and m'_b. The perturbation factor is only non vanishing for $m_a=m_b=m$ and $m'_a=m'_b=m'$ and is given by:

$$G^{NN}_{k_1k_2}(t) = \sum_{m,\,m'} [(2k_1+1)(2k_2+1)]^{\frac{1}{2}} \begin{pmatrix} I & I & k_1 \\ m' & -m & N \end{pmatrix}\begin{pmatrix} I & I & k_2 \\ m' & -m & N \end{pmatrix} e^{-\frac{i}{h}(E_m-E_{m'})t} \qquad (A.40)$$

For an axial symmetric field gradient with the energy differences $E_m-E_{m'}$ given by (A.37) the perturbation factor is:

$$G^{NN}_{k_1k_2}(t) = \sum_n S^{k_1k_2}_{nN} \cos(n\,\omega_0\,t) \qquad (A.41)$$

where n is a positive integer (including 0) with values $|m^2-m'^2|$ and $1/2|m^2-m'^2|$ for integer and half-integer I respectively. The coefficients $S^{k_1k_2}_{nN}$

$$S^{k_1k_2}_{nN} = \sum_{m,\,m'} [(2k_1+1)(2k_2+1)]^{\frac{1}{2}} \begin{pmatrix} I & I & k_1 \\ m' & -m & N \end{pmatrix}\begin{pmatrix} I & I & k_2 \\ m' & -m & N \end{pmatrix} \qquad (A.42)$$

For polycrystalline samples the angular correlation is obtained by averaging over all the directions of the microcrystals symmetry axes. The perturbation factor is given by:

$$G_{kk}(t) = \sum_n s_{kn} \cos(n\,\omega_0\,t) \qquad (A.43)$$

with

$$s_{kn} = \sum_{m,\, m'} \begin{pmatrix} I & I & k \\ m' & -m & -m+m' \end{pmatrix} \quad ; \; s_{00} = 1 \qquad \text{(A.44)}$$

where n has the same values as for (A.41). Numerical values for s_{kn} are tabulated for several values of the intermediate spin I in [Frauenfelder 65].

For a non-axial electric field gradient ($\eta \neq 0$) it is necessary to diagonalize the Hamiltonian H_{el} for each value of η. The perturbation factor can still be written as in (A.43) but the s_{kn} coefficients and transition frequencies depend on the value of η:

$$G_{kk}(t) = \sum_{n} s_{kn}(\eta) \cos(n_n(\eta)\, \omega_0\, t) \qquad \text{(A.45)}$$

n has the same restrictions as for (A.41), ω_0 is defined for $\eta=0$ and the dependence on the asymmetry parameter of the interaction frequencies is given by $n_n(\eta)$ ($n_0(\eta)=0$).

APPENDIX B

THE DATA ACQUISITION SYSTEM DEVELOPED IN COIMBRA

For the experiments developed in Coimbra a modular data acquisition system with several analog to digital converters (ADC) was built. A CAMAC histogrammic-memory (HM) controlled by a PDP 11/23 computer thru an appropriate interface is used to store the conversions. This system is easily and economically expanded by the addiction of more ADC's and histogrammic -memories.

The HM consits of a memory with 16k words (channels) 24 bits wide and a connection to an external ADC bus. In a Read-Increment cycle the HM receives a conversion address from the ADC bus and increments by one unit the corresponding word in it's memory. One important advantage of the use of this module is that, once initialized, it works independently of the CAMAC releasing the computer for use in other tasks.

As each experiment only requires 4k channels and the HM has 16k a digital router was built which divides the HM memory between four ADC's. This router receives the conversion addresses of up to four ADC's and sends them to the HM adding two routing bits to accumulate the ADC's conversions in different memory zones.

A block diagram of this system is represented in fig.B.1 where the connections to the PAC experiment are shown. It can be seen by this diagram that besides routing the four ADC's conversions the digital router allows routing bits from the experiment itself to be added to the ADC word before sending it to the HM. This subdivision of the ADC memory is particularly important in PAC experiments since 4 or 8 spectra (with 512 channels) are recorded simultaneously.

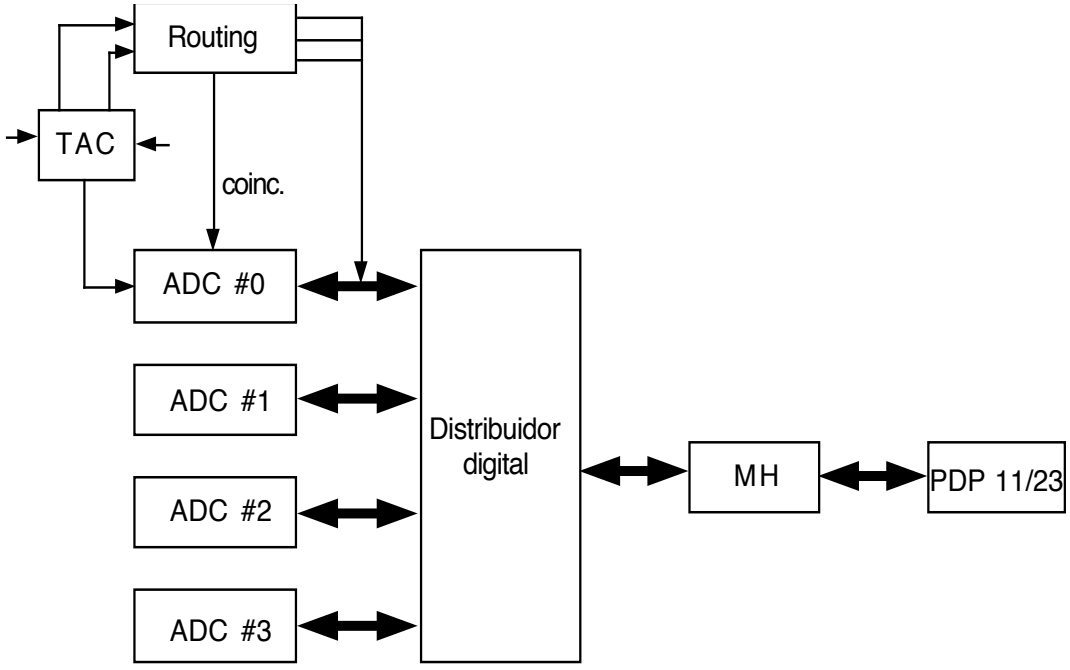

Fig. B.1- Block diagram of the data acquisition system developed in Coimbra with the connections to the PAC set-up shown. Routing— PAC routing module, TAC- time to amplitude converter ADC- analog to digital converter, DD- digital router, MH- histogramic memory.

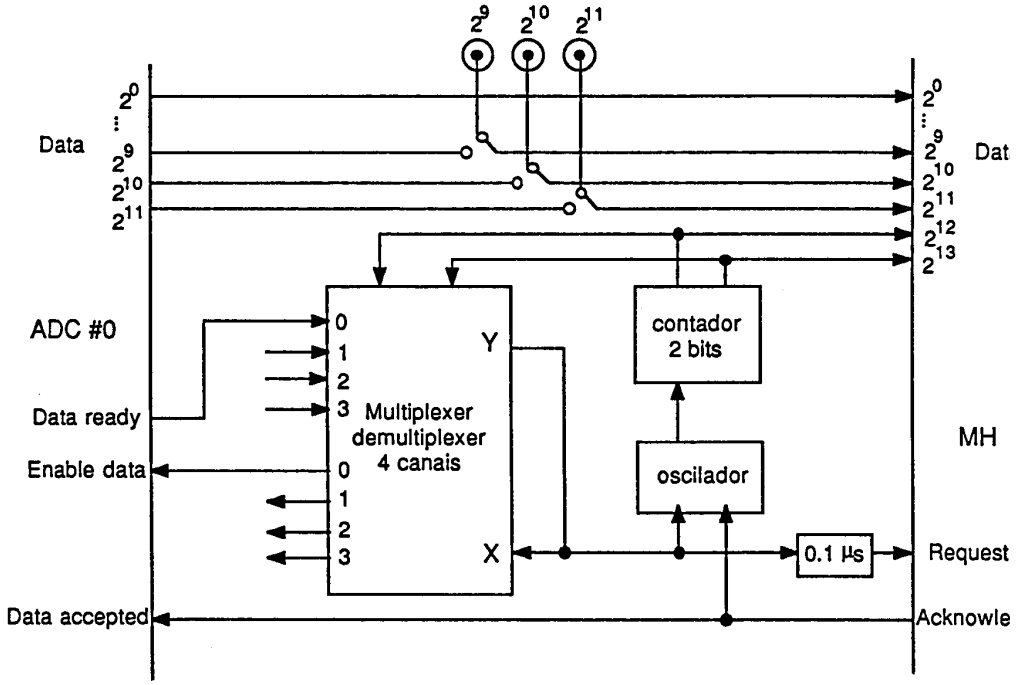

Fig.B.2- Block diagram of the digital router.

B.1 - The digital router

This module, whose block diagram is shown in fig.B.2, was based on a similar one described by Schemmerling et all [Schemmerling 83].

The digital router includes a 5MHz oscillator, a 2 bit counter and a digital multiplexer/demultiplexer. The counter is fed by the oscillator pulses and it's output is used to open the inputs and outputs of the multiplexer/ demultiplexer and as routing bits for the HM. Without conversions on the four ADC's a complete cycle needs approximately 0.8µs.

When ADC_i (i=0,1,2,3) has completed an analog to digital conversion it keeps the digitally encoded amplitude in an output register and sets it's Data Ready signal. When this signal is detected at input i in the multiplexer

it stops the oscillator via output Y. The same signal goes to input X of the demultiplexer and is fed via it's output i to the Enable Data of ADC_i causing it to send the output register contents to the address bus. The same Y signal, after a delay of 0.1μs is sent to the Request input of the HM initiating a Read-Increment cycle.

The HM receives 14 bits in it's address bus. Bits 0 to 11 correspond to the conversion of ADC_i and bits 12 and 13 correspond to the counter routing bits. After the Read-Increment cycle the HM sets it's Acknowledge signal which resets ADC_i and disconnects it from the address bus. This signal also restarts the oscillator after the Y signal has disappeared.

REFERENCES

Arends 80 - A.R.Arends, C.Hohenemser, F.Pleiter, H.de Ward, L.Chow and R.M.Sutter, Hyp. Int. 8 (1980) 191-213

Baker 73 - C.Baker and H.K.Birnbaum, Acta Metall. 21 (1973) 865-871

Bauer 75 - G.Bauer, E.Seitz, H.Horner and W.Schmtz, Sol.Stat. Comm. 17 (1975) 161-165

Bevington 69 - P.R.Bevington, "Data Reduction and Error Analysis for the Physical Sciences", McGraw Hill Book Company, 1969, New York

Bodenstedt 85 - E.Bodensteadt, Hyp. Int. 24/26 (1985) 521-537

Brigham 82 - E.O.Brigham, "FFT -Schnelle Fourier-Transformation", R. Oldenburg Verlag, 1982, München

Cannelli 85 - G.Cannelli, R.Cantelli and F.Cordero, Phys. Rev. B32 (1985) 3573-3579

Carstanjen 80 - H.D.Carstanjen, Phys. Stat. Sol. (a)59 (1980) 11-26

Carstanjen 82 - H.D.Carstanjen, Habilitation thesis, Universität München, 1982

Chen 76 - C.G.Chen and H.KBirnbaum, Phys. stat. sol. (a)36 (1976) 687-

Christiansen 76 - J.Christiansen, P.Heubes, R.Keitel, W.Klinger, W.Loefler, W.Sandner and W.Witthuhn, Z. Phys. B24 (1976) 177-187

Cost 84 - J.R.Cost, Acta Metall. 32 (1984) 123-130

Cotton 66 - F.Cotton, G.Wilkinson, "Advanced Inorganic Chemistry", John Wiley & Sons, New York, 1966

Dosch 85 - H.Dosch, U.Schubert, H.Metzger and J.Peisl, J. Phys. F14 (1984) 2467-2473

Feiock 69 - F.D.Feiock and W.R.Johnson, Phys. Rev. 187 (1969)39-50

Forker 73 - M.Forker, Nucl. Instr. Meth. 106 (1973) 121-126

Frauenfelder 65 - H.Frauenfelder and R.M.Steffen, in "Alpha-, Beta- and Gamma-ray spectroscopy", Vol 2, Cap.19, K.Siegbahn ed.,North-Holland Publ. Comp., Amesterdam, 1965

Fromm 80 - E.Fromm and G.Hörz, Int. Met. Rev. 5/6 (1980) 269-311

Gibala 85 - R.Gibala, J. Phys. Colloque C10-46 (1985) 43-46

Gil 84 - J.M.Gil, P.J.Mendes, C.Lopes Gil, A.P.de Lima, N.Ayres deCampos and A.Weidinger, J. Less Common Met. 103 (1984) 227-232

Gil 87a - J.M.Gil, P.J.Mendes, A.P.de Lima, N.Ayres de Campos, S.Yuquin, R.Peichl and A. Weidinger, J. Less Common Met. 129 (1987) 145-151

Gil 87b - J.M.Gil, Doctorate thesis, to be published

Hanada 77 - R.Hanada, Proc. 2nd Int. Conf. on Hydrogen in Metals, Paris, (Pergamon Oxford), Vol.3 (1977) 1B6

Hanada 81a - R.Hanada, M.Shinohara, Y.Sado and H.Kimura, J.Phys. Colloque C5 (1981) 757-761

Hanada 81b - R.Hanada, Scripta Metall. 15 (1981) 1121-1125

Hiraga 77 - H.Hiraga, T.Onozuka and H.Hirabayashi, Mat. Sci. Eng. 27 (1977) 35-

Kaim 79 - R.E.Kaim and D.W.Palmer, Philos. Mag. A40 (1979) 279-296

Kaufmann 79 - E.N.Kaufman and R.Vianden, Rev. Mod. Phys. 51 (1979)161-214

Lederer 78 - C.M.Lederer and V.S.Shirley eds., “Table of Isotopes”, 7ed., John Wiley & Sons Inc., 1978, New York

Locattelli 78 - M.Locattelli, K.Neumaier and H.Wipf, J. Phys. Colloque C6-39 (1985) 995-998

Magerl 83 - A.Magerl, J.J.Rush, J.M.Rowe, D.Richter and H.Wipf, Phys Rev B27 (1983) 927-934

Magerl 86 - A.Magerl, J.Dianoux, H.Wipf, K.Neumaier and I.S.Anderson, Phys. Rev. Lett. 56 (1986) 159-162

Mattas 75 - R.F.Mattas and H.K.Birnbaum, Acta Metall. 23 (1975 973-977

Matthias 63 - E.Matthias, W.Schneider and R.M.Steffen, Phys. Lett. 4 (1963) 41-43

Mendes 83 - P.J.Mendes, J.M.Gil, N.Ayres de Campos, R.Peichl and A.Weidinger, Hyp.Int. 15/16 (1983) 791-794

Mendes 85 - P.J.Mendes, J.M.Gil, N.Ayres de Campos, A.Weidinger and R.Peichl, Zeit. Phys. Chem. Neue Folge 145 (1985) 141-145

Metzger 76 - H.Metzger, J.Peisl and J.Wanagel, J. Phys. F6 (1976) 2195-2206

Metzger 85 - H.Metzger, U.Schubert and J.Peisl, J. Phys. F15 (1985) 779-797

Moffat 78 - W.G.Moffat, “The Handbook of Binary Phase-Diagrams”, Genum Publishing Company, New York, 1984

Morkel 78 - C.Morkel, H.Wipf and K.Neumaier, Phys. Rev. Lett. 40 (1978) 947-950

NDS 73 - Nuclear Data Sheets 9 (1973) 337

NDS 84 - Nuclear Data Sheets 43,3 (1984) 329

Okuda 84 - S. Okuda, H. Mizubayashi, N. Martsumoto, N. Kuramochi, C. Mochizuki and R. Hanada, Acta Metall. 32 (1984) 2125-2128

Nelson 75 - R.S.Nelson, “Radiation Damage Processes in Materials”, NATO Adv. Study Inst. Series E:Applied Sciences 8 (1975) 261-308

Pal 85 - B.Pal, J.Singh, S.D.Raj and S.Prakash, Phys. Stat. Sol. (b)129 (1985) 301-312

Peichl 83 - R.Peichl, A.Weidinger, E.Recknagel, J.M.Gil, P.J.Mendes and N.Ayres de Campos, Hyp. Int. 15/16 (1983) 463-466

Pfeiffer 76 - G.Pfeiffer and H.Wipf, J. Phys. F6 (1976) 167-179

Phillips 79 - M.E.Phillips and F.A.Smith, Nucl. Inst. Meth. 165 (1979) 83-90

Pleiter 73 - F.Pleiter, H.Bertschat, E.Recknagel and B.Spelmeyer, Nucl. Phys. A215 (1973) 471-476

Poker 79 - D.B.Poker, G.G.Setser, A.V.Granato and H.KBirnbaum, Zeit. Phys. Chem. Neue Folge 116 (1979) 39-45

Poker 84 - D.B.Poker, G.G.Setser, A.V.Granato and H.KBirnbaum, Phys. Rev. B 29 (1984) 622-629

Ponnambalam 84 - M.J.Ponnambalam and P.Jena, Hyp. Int. 20 (1984) 65-117

Ponnambalam 85 - M.J.Ponnambalam, J. Phys. F15 (1985) L7-L9

Prakash 85 - S.Prakash, Hyp.Int. 24-26 (1985) 491-519

Qi 82 - Zh.Qi, J.Völkl and H.Wipf, Scr. Metall. 16 (1982) 859-864

Recknagel 83 - E.Recknagel, G.Schatz and Th.Wichert, “Hyperfine Interaction of Radioactive Nuclei”, Cap.4, J. Christiansen ed., Topics in Current Physics, Springer Verlag, Berlin, 31 (1983) 133-204

Rosan 76 - K.Rosan and H.Wipf, Phys. Stat. Sol. (a)38 (1976) 611-620

Rose 67 - H.J.Rose and D.M.Brink, Rev. Mod. Phys. 39 (1967) 306-347

Rowe 80 - J.M.Rowe and A.Magerl, Phys. Rev. B21 (1980) 1706-1707

Sado 82 - Y.Sado, M.Shinohara, R.Hanada and H.Kimura, Proc. 3rd. Int. Congr. Hydr. in Mat., Paris, France, June 1982, pg.233-238

Schemmerling 83 - K.Schemmerling, J.Ahlert, M.Schumacher and F.Smend, Nucl. Instr. Meth. 216 (1983) 165-166

Schiller 75 - P.Schiller and H.Nijman, Phys.Stat. Sol. (a)31 (1975) K77-K79

Schubert 84 - U.Schubert, H.Metzger and J.Peisl, J. Phys. F14 (1984) 2457-2466

Schulze 77 - K.Sculze and H.Jehn, Zeit. Metallkd. 68 (1977) 654-660

Schulze 79 - K.Sculze, H.Jehne and E.Grallath, Zeit. Metallkd. 70 (1979) 625-630

Shakun 85 - N.A.Shakun, P.A.Svetashov and V.E.Storizhko, Radiat. Effects 90 (1985) 49-56

Shirley 83 - A.I.Shirley, C.K.Hall and N.J.Prince, Acta Metall. 31 (1983) 985-992

Smithels 67 - C.J. Smithells, “Metals Referenca Book”, Butterworth & Co., London, 1967, Vol II, pg.628

Takahashi 78 - J. Takahashi, M.Koiwa, M.Hirabayashi, S.Yamaguchi, Y.Fujino, K.Ozawa and K.Doi, J. Phys. Soc. Jap. 45 (1978) 1690-1696

Taylor 67 - A.Taylor and N.J.Doyle, J. Less Common Met. 13 (1967) 313-330

Vianden 83 - R.Vianden, Hyp. Int. 15/16 (1983) 189-202

Weidinger 79 - A.Weidinger, R.Wessner, Th.Wichert and E.Recknagel, Phys. Lett. 72A (1979) 369-372

Weidinger 81 - A.Weidinger, M.Deicher and T.Butz, Hyp. Int. 10 (1981) 717-720

Weidinger 85 - A.Weidinger and R.Peichl, Phys. Rev. Lett. 54 (1985) 1683-1685

Weller 85a - M.Weller, J. Phys. Colloque C10-46 (1985) 7-14

Weller 85b - M.Weller,I.Diehl, G.Hörz, R.Mann and K.Schulze, J. Phys. Colloque C10-46 (1985) 47-50

Wipf 81 - H.Wipf, A.Magerl, S.M.Shapiro, S.K.Satija and W. Thomlinson, Phys. Rev. Lett. 46 (1981) 947-950

Wipf 82 - H.Wipf and K.Neumaier, Proc. Int. Symp. on the Electronic Structure and Properties of Hydrogen in Metals, Richmond, USA, 1982

Wipf 84 - H.Wipf and K.Neumaier, Phys. Rev. Lett. 52 (1982) 1308-1311

Witthuhn 83 - W.Witthuhn and W Engel, “Hyperfine Interactions of Radioactive Nuclei”, Cap.5, Topics in Current Physics, J.Christiansen ed., Springer Verlag, Berlin, 31 (1983) 205-289

Wrede 86 - U.Wrede, T.Schaefer and R.Vianden, Zeit. Phys. B64 (1986) 461-467

Yates 65 - M.J.L.Yates, in “Alpha-, Beta- and Gamma-ray spectroscopy”, Appendix 9, Vol 2, K.Siegbahn ed., North-Holland Publ. Comp., Amesterdam, 1965

Zapp 80a - P.E.Zapp and H.K.Birnbaum, Acta Metall. 28 (1980) 1275-1286

Zapp 80b - P.E.Zapp and H.K.Birnbaum, Acta Metall. 28 (1980) 1523-1526